BULLETIN OF MAGNETIC RESONANCE

The Quarterly Review Journal of the International Society of Magnetic Resonance

VOLUME 19 May 1999 NUMBER 1/4

Proceedings of the International Society of Magnetic Resonance XIIIth Meeting Part I

Joint 29th AMPERE – 13th ISMAR

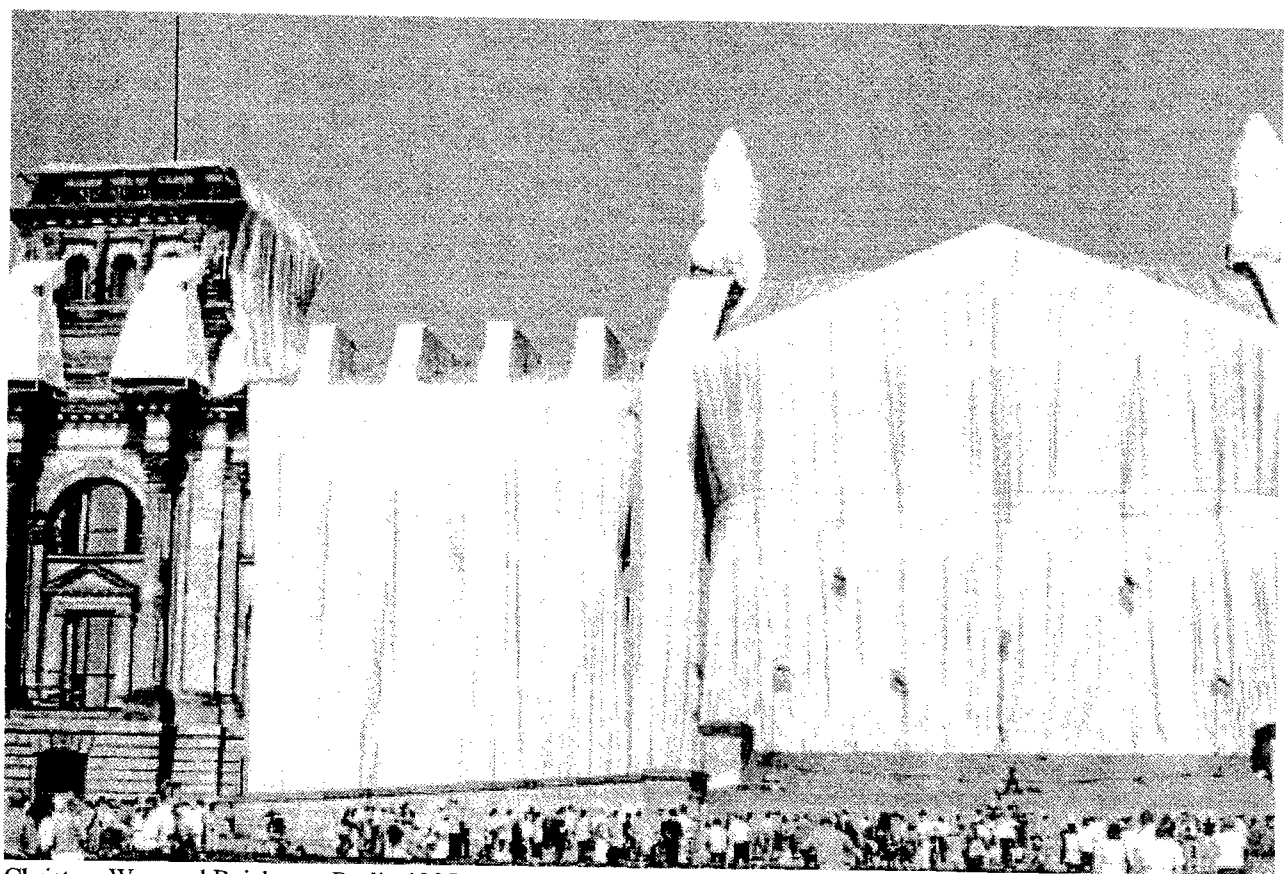

Christo – Wrapped Reichstag, Berlin 1995

International Conference on Magnetic Resonance & Related Phemonena

BULLETIN OF MAGNETIC RESONANCE

The Quarterly Review Journal of the International Society of Magnetic Resonance

---

The *Bulletin of Magnetic Resonance* is a quarterly review journal by the International Society of Magnetic Resonance. Reviews cover all parts of the broad field of magnetic resonance. viz.. the theory and practice of nuclear magnetic resonance, electron paramagnetic resonance, and nuclear quadrupole resonance spectroscopy including applications in physics, chemistry, biology, and medicine. The *BULLETIN* also acts as a house journal for the International Society of Magnetic Resonance.

CODEN: BUMRDT **ISSN: 0163-559X**

The aims of the International Society of Magnetic Resonance are to advance and diffuse knowledge of magnetic resonance and its applications in physics, chemistry, biology, and medicine, and to encourage and develop international contacts between scientists.

The Society sponsors international meetings and schools in magnetic resonance and its applications and publishes the quarterly review journal. The *Bulletin of Magnetic Resonance*, the house journal of ISMAR.

The annual fee for ISMAR membership is $20 plus $25 for a member subscription to the *Bulletin of Magnetic Resonance.*

Send subscription to:

International Society of Magnetic Resonance
Professor Regitze R. Vold, Treasurer
Department of Chemistry & Biochemistry
University of California, San Diego
9500 Gilman Drive
La Jolla, CA 92093-0359
(619) 534-0200; FAX (619) 534-6174
e-mail: rrvold@ucsd.edu

Joint 29th AMPERE - 13th ISMAR Conference

August 2-7, 1998, Berlin, Germany

Organizing Committee

D. Ziessow, Chairman
W. Lubitz, Co-Chairman
F. Lendzian, Secretary
D. Haberland, Local Organization

Program Committee

D. Ziessow, (Berlin)
W. Lubitz, (Berlin)
H. H. Limbach, (Berlin)
K. Möbius, (Berlin)
H. Oschkinat, (Berlin)
D. Stehlik, (Berlin)
B. Blümich, (Aachen)
K. P. Dinse, (Darmstadt)
C. Griesinger, (Frankfurt)
H. Günther, (Siegen)
A. Haase, (Würzburg)
U. Haeberlen, (Heidelberg)
H. Kessler, (München)
R. Kimmich, (Ulm)
G. Kothe, (Freiburg)
M. Mehring, (Stuttgart)
D. Michel, (Leipzig)
H. Rüterjans, (Frankfurt)
J.-M. Spaeth, (Paderborn)
H. W. Spiess, (Mainz)
D. Blechert, (Leipzig)

In consultation with

M. Goldman (France) President ISMAR
P. Servoz-Gavin (France) Secretary General ISMAR
B. Maraviglia (Italy) President Groupement AMPERE
R. Kind (Switzerland) Secretary General Bureau AMPERE

International Advisory Board
All members of the ISMAR Council and Committee AMPERE

CO-EDITORS OF THE PROCEEDINGS

D.G. Gorenstein
Department of HBC&G
Sealy Center for Structural Biology
Galveston, TX 77555-1157

D. Ziessow
Iwan-N.-Stranski-Institut
Berlin, Germany 10623

ACKNOWLEDGMENTS

The organizers are grateful to the following agencies, institutions, and companies for financial support:

Deutsche Forschungsgemeinschaft,
Deutsche Physikalische Gesellschaft/Heraeus-Stiftung,
Gesellschaft Deutscher Chemiker,
Deutscher Akademischer Austauschdienst,
Technische Universität Berlin,
Freunde des Weizmann-Instituts,
International Society of Magnetic Resonance,
Department of Energy (USA),
NMR Concepts (USA),
Bruker Analytik GmbH,
Schering AG Berlin,
Beiersdorf AG,
Martek Biosciences Corp. (USA),
Jeol GmbH Germany, and
Doty Scientific Inc. (USA)

1998 ISMAR PRIZE

The 1998 ISMAR prize was awarded to Ray Freeman in recognition of his pioneering developments of modern pulse techniques essential to applications in high resolution magnetic resonance spectroscopy. The prize was given to him at a ceremony during the 1998 ISMAR meeting in Berlin.

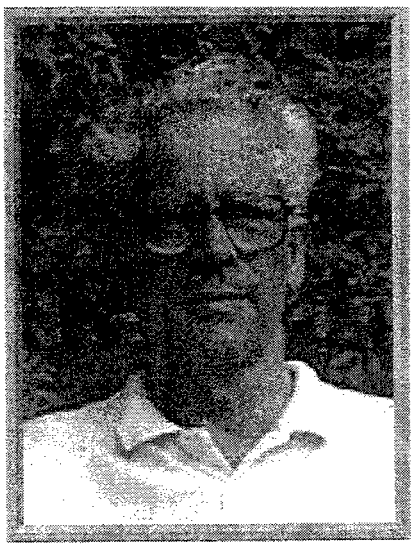

The International Society of Magnetic Resonance awards a prize every three years for outstanding achievement in the field of magnetic resonance. The previous winners of this prize are listed below.

1971 Erwin HAHN

1974 Herb GUTOWSKY

1977 Robert BLINC & E. K. ZAVOISKY

1980 Hans DEHMELT & Gunther LAUKIEN

1983 Anatole ABRAGAM & Brebis BLEANEY

1986 Charles SLICHTER

1989 John WAUGH

1992 Paul LAUTERBUR & Peter MANSFIELD

1995 Alfred G. REDFIELD

1998 Ray FREEMAN

Letter from the President

This Bulletin is dedicated to the Proceedings of the Joint 29th AMPERE - 13th ISMAR International Conference on Magnetic Resonance and Related Phenomena Berlin 1998

This Conference, chaired by Professor Dieter Ziessow and Wolfgang Lubitz, was a great success. Many thanks are due to the Organizers. More than 50 invited talks, 85 contributed papers, and 497 posters were presented by more than 730 participants. The ISMAR Prize was presented to Ray Freeman.

The next 14th ISMAR Conference will take place at Jerusalem in Israel in 2001, as approved by the ISMAR Council in Berlin. The year 2001 will mark the 30th Anniversary of the first ISMAR Conference, which took place in 1971, also in Jerusalem.

Professor David Gorenstein, Editor of the Bulletin of Magnetic Resonance since 1982, has stated his desire to retire from the editorship after the editing of this Bulletin.

The Bulletin was established in 1979/1980 by our first President, Professor Daniel Fiat. The Bulletin was first edited by Dr. Howard Bradbury and published with the Franklin Institute Press. In 1982, David Gorenstein was appointed as Editor, with publication by the University of Illinois. The fate of the Bulletin followed then David's tracks to Indiana and finally to Texas. More than 500 subscribers and over 100 university libraries took profit of the Bulletin over the years.

David Gorenstein deserves gratitude from the ISMAR Society for his outstanding contribution the Magnetic Resonance Community, as well as his staff, co-Editors, Editorial Board Members.

As you may know, Lyndon Emsley has established a web site http://www.ens-lyon.fr/ISMAR/ which is intended to host a Newsletter. You may wish to visit it if you have not done so already.

Clearly the future of ISMAR publications is now in question. Please communicate your thoughts on this issue.

As a (nearly) retiring President, I express my warmest wishes for a good health and a great future to ISMAR as well as to all practitioners of Magnetic Resonance, together with my hope of remaining on "speaking terms" with them until an unforeseeable future.

Maurice GOLDMAN
President of the ISMAR Society
Gif sur Yvette Cedex
FRANCE

Proceedings of the Joint 29th AMPERE and 13th ISMAR Conference

Part I

Contents

Optical Detection of Electron Paramagnetic and Electron-Nuclear Double Resonance of Point Defects in III-V Semiconductors

F. K. Koschnick
University of Paderborn, Physics Department, 33095 Paderborn, Germany
Tel: +49-5251-602748, Fax: +49-5251-603247, email: sp_fk@physik.uni-paderborn.de

Abstract: For the study of defects in III-V semiconductors an enhancement of sensitivity with respect to the conventional detection of electron paramagnetic and electron-nuclear double resonance (EPR/ENDOR) is necessary, because of low defect concentrations together with broad EPR lines and very small sample volumes as in the case of epitaxial layers. This can be achieved by optical detection of EPR and ENDOR (ODEPR/ODENDOR), which can be performed using optical absorption or luminescence. The first method is based on the measurement of a microwave or radio frequency induced change of the magnetic circular dichroism of the optical absorption (MCDA) and the second method detects the corresponding change of the intensity of the photoluminescence (PL) of a paramagnetic defect. Two examples of ODEPR/ODENDOR investigations in the III-V semiconductors GaAs and GaN are given. The investigations of the arsenic antisite-related (As_{Ga}-related) defects in GaAs were based on the MCDA-detection (MCDA-EPR/ENDOR), and the experiments on defects in GaN were performed via the PL-detection (PL-EPR/ENDOR). In GaAs several As_{Ga}-related defects can be measured. Three of them have almost undistinguishable EPR spectra. They can only be discriminated with MCDA and MCDA-ENDOR. The PL-EPR/ENDOR investigations on GaN were performed with a high frequency setup working at 72GHz. An enhancement in resolution and sensitivity was observed.

Keywords: GaAs, arsenic antisite defects, GaN, Mg-doping, Be-doping, ODEPR, ODENDOR, photoluminescence, MCDA

PACS: 76.70Hb, 78.55.Cr, and 67.80.Mg

1 Introduction

For the study of defects in III-V semiconductors an enhancement of sensitivity with respect to the conventional detection of electron paramagnetic and electron-nuclear double resonance (EPR/ENDOR) is necessary, because of low defect concentrations together with broad EPR lines and very small sample volumes as in the case of epitaxial layers. This can be achieved by optical detection of EPR and ENDOR (ODEPR/ODENDOR). Therefore, optical detection of EPR and ENDOR is a powerful tool to study paramagnetic defects in III-V semiconductors. It differs from conventional detection of EPR and ENDOR basically in that a microwave-induced repopulation of paramagnetic Zeeman levels is detected indirectly by a change in some property of light, which is either absorbed or emitted by the defect under study. The ODEPR/ODENDOR methods have a number of interesting features. One such feature is an enormous gain in sensitivity by several orders of magnitude due to a quantum transformation from 10^{10}Hz to 10^{15}Hz for detecting signals. Another interesting feature is the possibility of studying defects with a high selectivity. One of the problems of conventional EPR is the simultaneous presence of many paramagnetic defects, which renders the spectra very complicated. With optical detection every defect can be investigated separately, except for the rare situation that different defects have identical or extremely similar optical properties. In ODEPR the fact that magnetic sublevels can be selectively populated either by choosing appropriate experimental conditions or by physical mechanisms, such as spin selection rules for radiative or nonradiative transitions, plays an important role. Basically, the optical absorption or the luminescence of a defect can be used. Which of the techniques is applied, depends on the system and the kind of problem one wants to study.

After a short description of the basic ideas of the optical detection of EPR and ENDOR and the experimental setup, two examples for the successful application of ODEPR/ODENDOR on defects in III-V semiconductors are presented. The first example is the investigation of arsenic antisite-related defects (As_{Ga}-related defects) in GaAs which were investigated with ODEPR and ODENDOR based on the absorption technique, e.g., on the magnetic circular dichroism of the optical absorption (MCDA). The second example is related to the photoluminescence(PL)-detection of EPR and ENDOR of defects in GaN. In the following, MCDA-EPR and MCDA-ENDOR refer to the MCDA-detected EPR and ENDOR, and PL-EPR and PL-ENDOR refer to the photoluminescence-detection.

2 Experimental

a Detection via the MCDA

The MCDA is the differential absorption of right- and left-circularly polarized light, where the light is propagating along the direction of an externally applied static magnetic field $\mathbf{B_0}$. MCDA-EPR is measured as a

microwave-induced change of the MCDA. For a paramagnetic defect with S=1/2, the MCDA is proportional to the spin polarization of the ground state of the defect. For a high spin system (S>-1/2), this is also true, if the crystal field is small in comparison to the spin-orbit coupling of the ground and/or excited state. The MCDA is measured at high magnetic fields (1-3Tesla) and at low temperatures (1.5-4.2K), where the spin polarization of the ground state is large. In this paper only paramagnetic defects with S=1/2 are treated.

Upon inducing EPR transitions between the two ground state Zeeman levels of a S=1/2 system, the spin polarization is diminished if the EPR is (partially) saturated. This is monitored as a decrease of the MCDA [1]. MCDA-ENDOR is measured as an increase of the MCDA-EPR signal due to nuclear magnetic resonance (NMR) transitions induced simultaneously to the EPR transitions [1].

One can measure a kind of excitation spectrum of the MCDA-EPR/ENDOR lines. The ground state polarization is the same for all optical transitions of a certain defect. Therefore, one can set the EPR (ENDOR) resonance conditions to a particular EPR (ENDOR) line, vary the optical wavelength and monitor the EPR (ENDOR) signal intensity as the microwave-induced (radio frequency-(rf)-induced) change of the MCDA. Thus, from the total MCDA of a sample, only that part, which belongs to the EPR (ENDOR) line, will give a signal. This signal is called "tagged" MCDA [1].

b Detection via the photoluminescence

There are two types of recombination processes which are particularly suitable to serve as detection channels for EPR and ENDOR in semiconductors: the distant donor-acceptor pair recombination and the bound exciton recombination. The latter case leads to the optical detection of triplet states which are not discussed here. For a review see for example [2]. The investigations of GaN were performed via donor-acceptor recombinations (see below). If donors and acceptors are present in a semiconductor, most of the donors and acceptors are ionized depending on the position of the Fermi level E_F. If E_F is around mid gap, the donors have given up their electrons to the acceptors. In the ionized state donors and acceptors are diamagnetic. The donor-acceptor pairs are in the ground state. If the semiconductor is excited with light exceeding its band gap energy, electron-hole pairs are created. An electron may be trapped at a donor and a hole may be trapped at an acceptor forming a pair of a neutral donor and a neutral acceptor (excited state of a donor-acceptor pair). The neutral donor and the neutral acceptor are paramagnetic. If the concentration of the donors and acceptors are moderate, the average distance between a neutral donor and a neutral acceptor is large enough that the exchange interaction between them is weak. Due to the small coupling, the recombination probability of electrons with holes trapped at the donors and acceptors, respectively, is spin dependent. If the spin of the electron at the donor and that of the hole at the acceptor are parallel, the recombination

probability is small. If they are anti parallel, it is large. Because of the different spin-dependent recombination probabilities depending of the pairs spin state, the intensity of the donor-acceptor pair recombination luminescence can be used as a detection channel for EPR and ENDOR. Because the exchange interaction between the separated spins is weak, the photoluminescence detection reveals the EPR and ENDOR signals of each of the paramagnetic species separately, allowing direct identification of the two partners.

The sample is placed in an external magnetic field and exposed to excitation light creating the electron-hole pairs. Microwaves induce spin flip transitions in the excited states of the donor-acceptor pairs transferring population from the parallel to the anti parallel donor acceptor spin states, where the recombination probability is larger. In the case of ENDOR, a rf field is applied to the sample simultaneously to the microwaves. The change in the intensity of the donor-acceptor pair recombination luminescence is a measure for the EPR or ENDOR effect. Usually, this effect is luminescence enhancing. In solids, the relative change of the luminescence intensity due to EPR and ENDOR is between 10^{-2} and 10^{-5}. For further details of this method see for example [3].

c Experimental setup

The experiments were performed using a custom-built K-band spectrometer (24GHz), which is able to measure optical detection via the MCDA and via the PL. In figure 1, a schematic diagram of the setup is

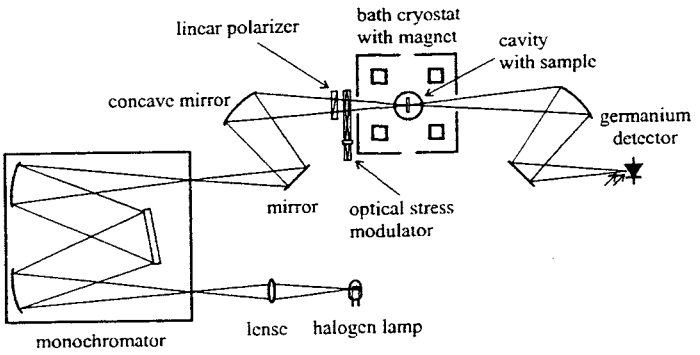

Figure 1: Schematic diagram of the ODEPR/ODENDOR spectrometer. Optical detection can be performed with MCDA or with PL. The microwave and radio frequency setup is not shown. Using a germanium detector, the spectral range of the spectrometer is 0.7-2.0eV. For details see text.

shown. The light of a halogen lamp is dispersed by a monochromator. For MCDA measurements a linear polarizer and a piezo-electric driven optical stress modulator produces the left- and right-circular polarization of the light. The stress modulator is an "oscillating (/4 plate", the variation of (being achieved by the stress amplitude. For PL-EPR/ENDOR experiments the polarizer and the modulator are removed. In such a case the halogen lamp and the monochromator are used as an excitation source. In particular, this kind of excitation was performed for the investigations on GaN. It turned out that a laser was not suitable for PL-EPR/ENDOR measurements on GaN because of the high noise level in the time regime of the modulation and integration performed in the experiments.

The sample is located in a special cylindrical TE_{011} microwave cavity with optical access. The cavity is placed inside a liquid helium bath cryostat. Inside the cavity, there are four ENDOR rods parallel to the cavity axis, which act as a pair of rf coils producing the rf field for the NMR transitions at the sample position.

A superconducting magnet produces the external magnetic field. A cooled germanium detector or a photomultiplier is used to measure the transmitted (MCDA) or emitted (PL) light.

The MCDA is detected with lock-in technique, the reference frequency being the eigen frequency of the stress modulator (30kHz). Usually, the microwaves and/or the rf are not modulated in a MCDA-EPR/ENDOR experiment.

In the case of PL-EPR/ENDOR measurements, the integral (total) PL intensity is measured. Occasually, the PL light is dispersed with a set of optical filters. Usually, the spectral resolution is larger than the width of the investigated PL bands, typically of width of (0.1-0.3eV. PL-EPR/ENDOR is measured as a change of the PL intensity with amplitude modulation of the microwaves or rf, respectively, and lock-in technique.

For sensitivity enhancement of MCDA and MCDA-EPR/ENDOR measurements a mirror cavity can be used [4]. In figure 2 such a cavity, in which the optical beam passes through the sample several times, is shown. The operation of the cavity is based on the idea that the phase shift of (of the circular polarization of the reflected light is compensated by the phase shift

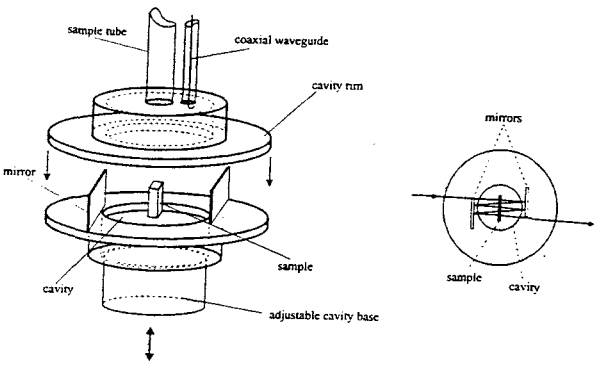

Figure 2: Mirror cavity for sensitivity enhancement of MCDA-based measurements. On the left side is the schematic diagram of the mirror cavity. The distance between the upper and lower part of the cavity is increased which allows a clear view. Right: top view with a four fold reflection of the light beam.

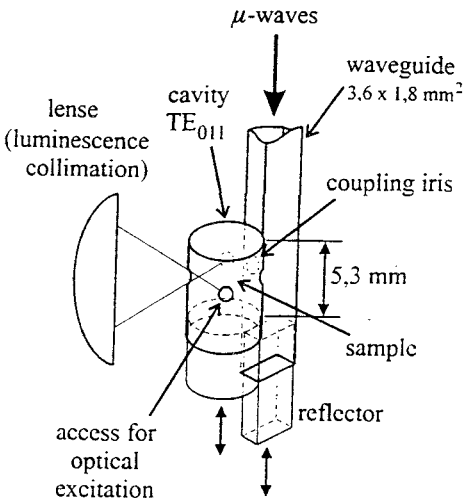

Figure 3: TE_{011} cavity for 72GHz (V-band) with optical access.

of the MCDA when the light beam is traveling in the opposite direction with respect to the magnetic field. In this way the contribution of each reflection

to the total MCDA signal is positive, and the MCDA enhancement is nearly proportional to the number of passages of the light beam through the sample.

An increase in the resolution and also an increase of the sensitivity in PL-EPR/ENDOR can be achieved with a high microwave frequency setup working at 72GHz (V-band). In particular, this setup was used for the PL-EPR/ENDOR investigations of GaN (see below). The 72GHz cavity is depicted in figure 3. Due to the magnetic field, which is three times larger using the V-band in comparison to the K-band, the resolution for the discrimination of different defects with slightly different g-values obtained in PL-EPR experiments was three times larger. In addition, a sensitivity enhancement in the PL-EPR/ENDOR measurements on GaN was observed (see below). For further experimental details the reader is referred to [1].

3 MCDA-detected EPR and ENDOR on As_{Ga}-related defects in GaAs

GaAs is one of the most used semiconductor materials. Its direct band gap and high electron mobility lead to many applications where high speed or infrared light are involved, e.g., fast digital circuits and laser diodes. The electrical and optical properties of GaAs are influenced by intrinsic defects.

The most prominent intrinsic defect in GaAs is the EL2 defect, a deep As_{Ga}-related double donor, which is responsible for the semi-insulating (SI) character of nominally undoped, as-grown GaAs. By irradiation with high energy electrons intrinsic defects like As_{Ga}-related defects can be artificially produced in concentrations which allow their investigation using magnetic resonance techniques, such as the MCDA, MCDA-EPR, and MCDA-ENDOR. A whole family of As_{Ga}-related defects has been identified [5]. At least three As_{Ga}-related defects different from the EL2 are formed by electron irradiation of GaAs.

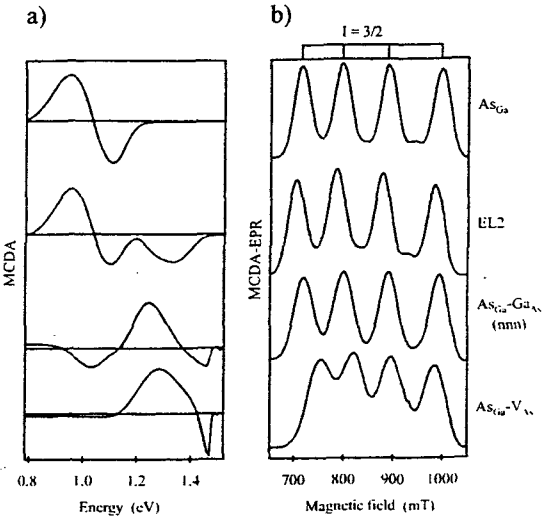

Figure 4: (a) "tagged" MCDA spectra and (b) MCDA-EPR spectra of four different As_{Ga}-related defects. The spectra of the four different As_{Ga}-related defects were recorded in different GaAs samples. The isolated As_{Ga} was measured in SI GaAs which was irradiated with 2MeV electrons at 4.5K and kept below 77K. The EL2 defect was measured in as-grown SI GaAs. The anti-structure pair [As_{Ga}-Ga_{As} (nnn)] was observed in SI GaAs electron irradiated at 4.5K and annealed to room temperature (RT), and the As_{Ga}-V_{As} defect was measured in Te-doped, at 4.5K electron-irradiated GaAs which was annealed to RT. Measurement temperatures 1.5K, microwave frequency 24GHz

In figure 4 the "tagged" MCDA and the MCDA-EPR spectra of four As_{Ga}-related defects, the EL2 defect and three electron irradiation-induced defects are shown. The four different As_{Ga}-related defects were measured in samples with different preparation conditions (see caption of figure 4). The MCDA-EPR spectra of the four As_{Ga}-related defects show the typical four-line pattern of the resolved hyperfine(hf)interaction of the central ^{75}As nucleus with a nuclear spin of I=3/2. Three of these As_{Ga}-related defects have hf splittings which are almost undistinguishable. The isotropic hf splittings are approximately 2600-MHz. These defects are called "the antisites with the large hf interaction". One defect (see lowest MCDA and MCDA-EPR spectrum in figure 4), has an isotropic hf interaction of only 2050-MHz ("antisite with the small hf interaction").

From the MCDA-EPR spectra alone, it was not possible to analyze the detailed microscopic structures of the respective defects. The high abundance of magnetic isotopes with nuclear spin of I=3/2 of both lattice atoms in GaAs causes a large inhomogeneous broadening of the hf split EPR lines preventing the resolution of the superhyperfine (shf) interactions, i.e., the magnetic interactions between the unpaired electron spin and the nuclear spins of the neighbor nuclei. The resolution of the shf interactions is needed to establish a microscopic model [1]. ENDOR can resolve these shf interactions. The microscopic structures of the As_{Ga}-related defects were investigated using MCDA-ENDOR, which is more sensitive than conventional ENDOR, which was not successful for sensitivity reasons [5,6]. Two of the large As_{Ga}-related defects were attributed to the isolated As_{Ga} defect and an anti-structure pair [$As_{Ga}Ga_{As}$ (nnn), i.e., an As_{Ga} with a Ga antisite (Ga_{As}) in the next nearest neighbor position] [5]. The EL2 defect is believed to be a complex consisting of an As_{Ga} and an arsenic interstitial in the neighborhood. The As_{Ga}-related defect with the reduced hf splitting compared to the other three As_{Ga}-related defects mentioned above was attributed to a As_{Ga}-V_{As} complex, an As_{Ga} with an arsenic vacancy (V_{As}) in the direct neighborhood [6]. As an example, its MCDA-ENDOR spectrum is shown in figure 5. The detailed ENDOR analysis can be found in [6].

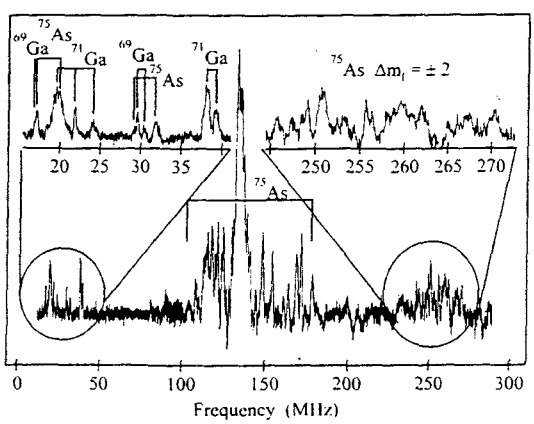

Figure 5: MCDA-ENDOR spectrum of the As_{Ga}-V_{As} defect at T=1.5K. The photon energy was 1.287eV, the magnetic field was 830mT, the microwave frequency was 24.01GHz, the angle between the static magnetic field and the [100] direction was 30° and between the [110] direction was 90°. The total measurement time for this spectrum was 10h.

Table 1: Shf and quadrupole data of the first arsenic neighbor shell of the As_{Ga}-related defects in GaAs as determined by MCDA-ENDOR after [5,6]. For the anti-structure pair [As_{Ga}-Ga_{As} (nnn)] two sets of parameters were measured because of the splitting of the first arsenic shell into two subshells [5]. The angles β_B and β_Q are the Euler angles which describe the orientations of the shf and quadrupole tensors, respectively. 54.74° means that the z-axis of the tensors are parallel to a <111> direction.

As_{Ga}-related defect	a / h (MHz)	b / h (MHz)	β_B (degree)	q / h (MHz)	β_Q (degree)
EL2	169.3	53.2	54.74	11.7	54.74
As_{Ga}	169.3	53.9	54.74	12.0	54.74
As_{Ga}-Ga_{As}	158.5	54.7	54.74	12.9	54.74
(nnn)	205.4	50.8	54.74	11.1	54.74
As_{Ga}-V_{As}	252	24	70	0.9	165

The shf and quadrupole data of the first arsenic shells of the four discussed As_{Ga}-related defects are collected in table 1. The shf interaction is described with a shf interaction tensor $\underline{A}$. Assuming axial symmetry, its principal values in its principal axes system are A_{xx}=a-b, A_{yy}=a-b and A_{zz}=a-+2b, where a is the isotropic Fermi contact term and b is the anisotropic shf parameter [1]. The quadrupole interaction is described with the tensor $\underline{Q}$. Its principal values in the principal axes system are Q_{xx}=-q, Q_{yy}=-q, Q_{zz}=2q (axial symmetry) [1]. The shf interaction parameters are a measure of the unpaired spin density distribution of a defect. The parameter q is a measure of the electric field gradient at the respective neighbor nucleus [1]. From table 1 can be clearly seen that the shf interaction and quadrupole parameters of the isolated As_{Ga} and those of the EL2 are very similar. Therefore, the spin density distributions of both defects at the central As_{Ga} atom and its direct neighborhood and the electric field gradient at the first arsenic shell of both defects must be very similar. This is very surprising because the defects are different and have different optical properties. It is not understood why the excited states (optical properties) are so much different in spite of the similarity of the ground states (spin density distribution) of the defects. The As_{Ga}-V_{As} defect has very much different parameters. This is probably due to the perturbation of the arsenic vacancy in the first arsenic shell. In the case of the EL2 defect and the anti-structure pair the interstitial arsenic atom and the gallium antisite, respectively, are located in shells which are further away from the central As_{Ga} atom.

4 PL-detected EPR and ENDOR on defects in GaN

Strong efforts on the synthesis and device aspects of GaN took place in the past few year for the realization of blue lasers and LEDs. Progress was

hampered because of several severe materials problems. One of these problems was the high residual n-type conductivity of hetero-epitaxial GaN layers (10^{17}-10^{19}cm^{-3}). GaN has to be grown with epitaxy. (Bulk growth is only possible under extreme conditions, pressures of about 2GPa. and temperatures of about 1700°C [7].) The substrates used for hetero-epitaxy of GaN have a large lattice mismatch. Mostly, sapphire, GaAs or Si are used as substrates. In nominally undoped state-of-the-art material, the concentration of residual shallow donors is now in the 10^{16}cm^{-3} range. Recently, two shallow donor levels at approx. 22 and 34meV below the conduction band edge were reported [8]. But the origins of the residual donors are still unclear. Another problem which hampers the development of photonic devices is the difficulty in achieving a high p-type doping level. The most used dopant for p-type doping is Mg. But Mg induces deep complex defects at high doping levels preventing large hole concentrations (n_p) in the valence band at room temperature (n_p(-10^{17}cm^{-3}). Another approach is Be-doping to achieve p-type conductivity. But like Mg, Be induces also deep complexes at high doping levels. It was the purpose of this study to examine whether different donors and acceptors (Mg-related and Be-related) can be discriminated with the high resolution of a V-band set-up.

In contrast to GaAs, where the optical detection of magnetic resonance was performed via an absorption method, GaN had to be investigated using the luminescence-detection, since GaN is only available as very thin (1-μm-10μm) hetero-epitaxial layers, in which the absorption is too weak. Luminescence-detected magnetic resonance investigations were performed on nominally undoped, Mg-doped, and Be-doped GaN. For enhanced resolution and sensitivity, the V-band set up was used. With the typical microwave power of about 100-mW and with the typical power of the excitation light of 0.1mW at the sample, the PL-EPR effects in GaN were of the order of 10^{-3} or less of the total luminescence intensity. The PL-EPR spectra of the nominally undoped samples were measured via the well-known "yellow luminescence" [9-12], those of the Mg-doped samples were measured via the blue Mg-related luminescence around 2.9eV [13] and those of the Be-doped samples via the deep Be-induced luminescence around 2.4eV [14]. The nominally undoped and Mg-doped GaN samples were grown with metal organic vapour phase epitaxy (MOVPE) on sapphire. The Be-doped material was grown with molecular beam epitaxy (MBE) on Si. The nominally undoped samples had residual n-type carrier concentrations at room temperature in the 10^{16}cm^{-3} range. The Mg-doped samples were measured before and after annealing in a nitrogen atmosphere at 650°C for 30 minutes. This annealing is necessary to activate the acceptors which are believed to be passivated by hydrogen in as-grown material [15,16]. The Mg concentrations of the samples varied from 10^{18}cm^{-3} to 3(10^{19}cm^{-3}. The hole concentrations were in the 10^{16}cm^{-3} to

$10^{17}cm^{-3}$ range at room temperature after activation. The samples with the low doping level were highly resistive. The undoped samples and the Mg-doped samples were supplied from the CRHEA-CNRS in Valbonne. The Be-doped MBE-grown samples were supplied from the University of Madrid. No reliable Hall data could be obtained on the Be-doped samples because of interdiffusion of Ga from the layer into the Si substrate during growth [17].

a) PL-EPR/ENDOR measurements via the "yellow luminescence" in undoped GaN

The yellow luminescence is believed to be caused by pair recombinations between residual, shallow donors and deep acceptors having their electrical levels approx. 1-eV above the valence band edge [9,11,12]. In this luminescence, three resonances labeled (a)-(c) in figure 6 were observed. The resonances (a) and (c) are well-known and were recently attributed to a deep defect ($g_{||}$=1.989) and to a residual shallow donor ($g_{||}$=-1.952) [10], respectively. Due to the higher resolution of the PL-EPR in the V-band compared to the previous measurements [10] the resonance labeled (b) could be resolved. It is usually hidden underneath (a) and (c), when using K- or Q-band microwave sources (24GHz and 36GHz). Within experimental error, resonance (b) shows no anisotropy. Its g-value and half width are: g=1.958±0.001 and ($B_{1/2}$(-25mT. From the g-value, it is inferred that this resonance is caused by a donor-like defect, probably a shallow one. This observation indicates that the yellow luminescence is caused by recombination processes where at least two different shallow donors are involved. It is speculated that the two shallow donor levels reported in [8] belong to the same two defects responsible for the two shallow donor-like resonances (b) and (c) shown in figure 6.

In figure 7 PL-ENDOR spectra of the residual, shallow donor measured with K- and V-band are shown. Clearly, it can be seen that the V-band spectrum has a much better signal-to-noise ratio compared to that of the K-band. The increase in sensitivity was about one order of magnitude. The ENDOR lines arise from the two gallium isotopes ^{69}Ga (abundance 60%, I=3/2) and ^{71}Ga (abundance 40%, I=3/2). The splitting is due to a quadrupole interaction [18]. From the quadrupole interaction the electric field gradient at the gallium nuclei was estimated to be (6.5±0.2)(-$10^{20}Vm^{-2}$ [18]. This value comes close to the intrinsic electric field gradient at a regular gallium lattice site determined from magic angle sample-spinning nuclear magnetic resonance (MASS-NMR) on GaN powder [19]. Unfortunately, hf or shf interactions could not be resolved with PL-ENDOR. Probably, these interactions are hidden within the widths of the ENDOR lines. From the angular dependence of the ENDOR line positions and widths, it was speculated that the residual donor is

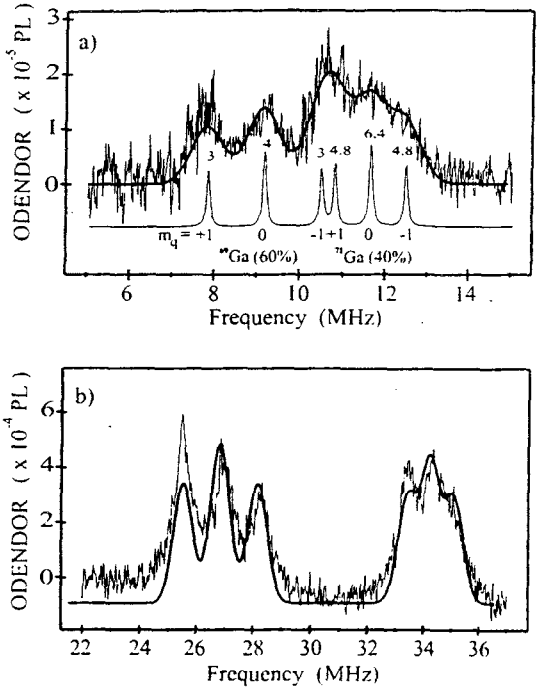

Figure 7: PL-ENDOR spectra of the residual, shallow donor in MOVPE-grown GaN measured in the yellow luminescence at 1.5K with the magnetic field parallel to the hexagonal c-axes. The photon energy of the excitation was 3.75eV. The ENDOR lines are due to the two gallium isotopes ^{69}Ga and ^{71}Ga. (a) K-band spectrum, microwave frequency 24GHz, resonance field 0.874T, recording time 5h, (b) V-band spectrum, microwave frequency 72.73-GHz, resonance field 2.65T, recording time 1/2h. The black solid lines are calculated ENDOR spectra with the assumption of a quadrupole interaction of q=0.22MHz and a line width of approx. 0.8MHz. The calculated spectrum with the small line width in (a) shows the positions and the relative intensities of the individual ENDOR lines. Hf (hyperfine) or shf (superhyperfine) interactions could not be resolved.

a gallium interstitial and that the gallium ENDOR lines shown in figure 7 are caused by the central gallium atom of the defect [18]. The gallium interstitial was calculated to be a shallow donor [20, 21]. On the other hand, assuming this model it is not easily understood why the electrical field gradient at the interstitial position is similar to that of the regular unperturbed gallium lattice site.

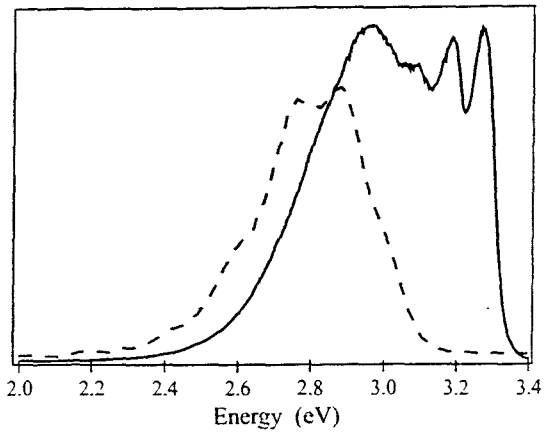

Figure 8: Photoluminescence spectra of Mg-doped GaN, excited with a HeCd laser at 1.5K. Solid line: sample with a lower Mg-doping level (10^{18}-10^{19}cm^{-3}), broken line: sample with a high Mg-doping level (more than 10^{19}cm^{-3}). The structure on the luminescence band is believed to be caused by two overlapping donor acceptor pair recombination bands with replica [22].

b) PL-EPR measurements via the blue Mg-related luminescences in Mg-doped GaN

Figure 8 shows the blue Mg-related luminescences observed in two

different Mg-doped GaN samples. The Mg-related luminescence of the sample with the larger Mg-doping level is shifted to lower photon energies. It is believed that this red shift of approximately 300meV is caused by the formation of deep Mg complexes at larger doping level. This formation limits the concentration of shallow Mg acceptors obtained by the doping.

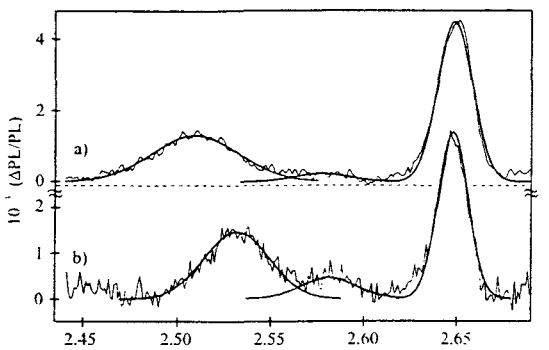

Figure 9: PL-EPR spectra recorded at T=1.5K with the magnetic field parallel to the hexagonal c-axis, microwave frequency 72.73GHz, excitation at 3.65-eV, curve (a) Mg-doped sample with a large doping level (more than $10^{19}cm^{-3}$), (b): Mg-doped sample with a low doping level (10^{18}-$10^{19}cm^{-3}$), the Gaussians represent the deconvolution, parameters see text.

In the Mg-doped samples we observed several resonances, probably Mg-related, and a dominant signal at 2.65T for **B**||**c** ($g_{||}$=1.960(0.003, see figure 9), which probably belongs to donor-like defects. The half width of this resonance is approx. 23mT. The line shape shows a slight asymmetry. Therefore, it is possible that this signal is a superposition of several signals. It can be concluded from the g-values and the half width of the donor-like signal that in the Mg-doped samples the donors must be different from the residual donors observed in undoped material [signal (c) in figure 6]. It can not yet be decided whether the new shallow donor resonance observed in undoped material [labeled with (b) in figure 6] is identical with the resonances in as-grown Mg-doped material. To make sure that the differences in the g-values and half widths of the donor-like resonances between Mg-doped and undoped GaN is not caused by exchange interactions between the donors and Mg-acceptors in the highly doped samples, we changed the intensity of the excitation light by a factor of ten. No changes in the PL-EPR spectra due to the variation of the excitation light intensity were detected. Therefore exchange interactions between the donors and the Mg acceptors are not responsible for the different measured g-values and half widths. The Mg-doping has definitely an influence on the donors created. Whether this is due to impurities which might be incorporated into the sample or whether it is caused by a process of self compensation is not yet clear.

The resonances observed below 2.6T in all investigated Mg-doped samples are probably related to Mg-type defects because they were never observed in undoped samples. In the samples with the high Mg-doping level

($3(10^{19}cm^{-3})$ two Mg-related resonances were observed (curve (a) in figure 9) with $g_{||}=2.07(0.005$, $g_{(}=2.03(0.005$, ($B_{1/2}=45mT$ and $g_{||}=2.02(0.005$, $g_{(}=-2.00(0.005$, ($B_{1/2}=35mT$. The first resonance is similar to that observed by Glaser et al. and Kunzer et al. [10,23] and what was assigned to a deep Mg-related complex. Neither resonance was influenced by the annealing process (activation). Therefore, it is concluded that these Mg-related defects are not responsible for the p-type conductivity after activation. In the sample with the lower doping level ($10^{18}cm^{-3}$) not only a different PL spectrum was observed in comparison to the samples with the high doping level, but also a different Mg-related PL-EPR resonance was measured (figure 9, curve (b), $g_{||}=2.057$-(0.005, $g(=2.045(0.005$ and ($B_{1/2}=45$-mT). A second Mg-related resonance was identical within experimental error with the $g_{||}=2.02$ signal in the samples with the high doping level. The observation of different PL bands and different Mg-related resonances in samples with different Mg-doping level indicates that different Mg-related deep defects can be formed in GaN depending on the Mg concentration. The g-anisotropy of shallow Mg acceptors is expected to be large [10], much larger than those observed in the experiments. Therefore, it is reasonable to conclude that deep Mg-related defects were measured.

c) PL-EPR measurements via the 2.4eV Be-related luminescences in Be-doped GaN

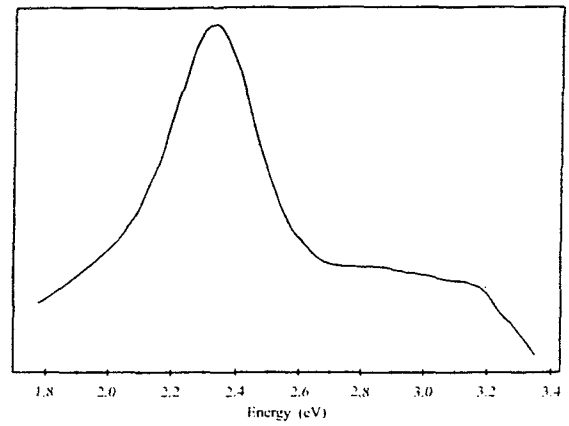

Figure 10: PL-spectrum of the Be-doped MBE-grown GaN sample, substrate Si, excitation with an argon-ion-laser (355nm), temperature 1.5K.

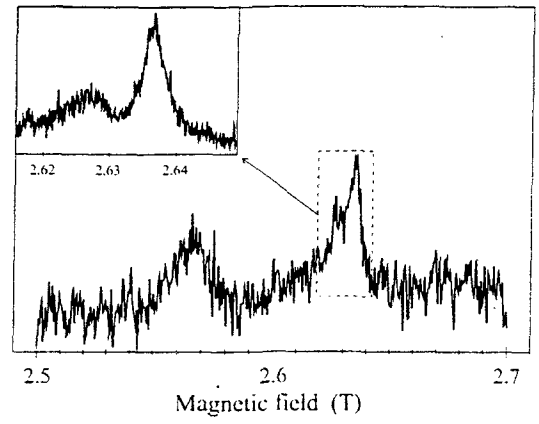

Figure 11: PL-EPR spectrum of the Be-doped MBE-grown GaN sample, measured in the 2.4eV luminescence (see figure10), the spectra were measured at 72.73GHz and at 1.5K, B||-c-axis. The inset shows the two donor-like resonances. The broad signal around 2.55T is believed to be a deep Be-related acceptor.

The PL spectrum of a Be-doped sample is shown in figure10. With PL-EPR (figure 11), an isotropic resonance with g=2.008(0.003 at 2.58T was observed which is acceptor-like, inferred from its g-value. This resonance is most probably due to Be-related defects. Because it was measured via the deep luminescence band we believe that those Be-related defects are deep complexes. For shallow acceptors a strong g-anisotropy would be expected.

Two donor-like resonances at higher fields (around 2.65T) were measured. The two resonances are shown in the inset of figure 11 with higher resolution. The resonance at higher fields has the same half width and the same g-values as measured for the shallow donor labeled with (c) in figure 6 ($B_{1/2}$=7mT, $g_{||}$=1.955(0.001, $g_{\perp}$=1.949(0.001). The other weaker resonance at lower fields has only a very small anisotropy. Its EPR parameters are: $B_{1/2}$=15mT, $g_{||}$=1.956(0.001, $g_{\perp}$=1.957(0.001. We believe that this second resonance is also caused by a donor, probably a shallow one. Therefore, two donors are present in MBE material. One of them is identical to a shallow donor observed in nominally undoped MOVPE-grown GaN. MBE growth was performed with high purity solid sources ((7N) for Ga and Be and with high purity N_2 gas. Impurities other than the dopant Be and the substrate material Si are not expected to be present in the samples in a concentration which is measurable with PL-EPR. Therefore, the donors could be due to Si or intrinsic defects. With SIMS measurements, a diffusion of Si into the GaN layer was observed [17]. Oxygen can be excluded, because it is not present as a contamination source in MBE growth. Whether the Be-doping has an indirect influence on the creation of donors, could not be investigated, because it was not possible to measure PL-EPR on nominally undoped MBE samples.

5 Conclusion

Two examples of the successful application of optical detection of EPR and ENDOR on III-V semiconductors were presented. GaAs was investigated with MCDA-detection, a detection scheme based on optical absorption. It was shown that the detailed microscopic structure of four As_{Ga}-related defects could only be analyzed with the MCDA-ENDOR technique. The three antisites with the large hf interaction, the isolated As_{Ga}, the EL2 and the anti-structure pair, have hf splittings which are almost identical. The shf parameters of their first arsenic shells are very similar in contrast to the fact that the optical properties (MCDA bands) are very different. Up to now this behavior is not understood. The fourth antisite, the As_{Ga}-V_{As}, has different parameters in comparison to the antisites with the large hf interaction. This can be explained with the strong perturbation due to the arsenic vacancy in the first arsenic shell. In the case of the EL2 and of the anti-structure pair the complex partners (perturbations) of the central

As_{Ga} atom are not in the direct neighborhood.

With PL-EPR measurements in the V-band on GaN new defects were detected which cannot be seen with K- and Q-bands because of less resolution there. Probably new different shallow donors were detected in undoped and Be-doped GaN. In Mg-doped GaN the donors are different from those in undoped GaN. It is not yet clear whether this is an effect of self compensation or of incorporation of impurities along with the Mg-doping. Several defects, probably Mg-related, were detected. They are deep defects and probably not related to the Mg-acceptors giving rise to the p-conductivity. Similar to Mg, Be also forms deep acceptors.

Acknowlegdement:

The author wishes to acknowledge Prof. Dr. J.-M. Spaeth for numerous and insightful discussions.

The investigation on GaAs was supported by the Deutsche Forschungsgemeinschaft, Grant No. Sp189/35-1. The electron irradiation was performed at the Forschungszentrum Jülich.

The work on GaN was supported by the project, Esprit "LAQUANI", Grant No. 20968 of the European Union. The investigated GaN samples were supplied from the Centre de Recherche sur l'Hétéro-Epitaxie et ses Applications (CRHEA-CNRS) in Valbonne (France) and from the University of Madrid.

References:

[1] J.-M. Spaeth, J. R. Niklas, and R. H. Bartram: "Multiple Magnetic Resonance Spectroscopy for Structural Analysis of Point Defects in Solids", Springer, Heidelberg 1992

[2] W. B. Lynch and O. W. Pratt, *Magn. Res. Rev. (GB)* **10**, 111 (1985)

[3] B. C. Cavenett, *Adv. In Phys.* **30**, 475 (1981)

[4] F. K. Koschnick, *Rev. Sci. Instrum.* **68**, 2511 (1997)

[5] J.-M. Spaeth and K. Krambrock, *Adv. in Solid State Phys.* **33**, 111 (1993)

[6] F. K. Koschnick, K.-H. Wietzke, and J.-M. Spaeth, *Phys. Rev. B* in press (1998)

[7] J. Karpinski, J. Jun, and S. Porowski, *J. Crystal Growth* **66**, 1 (1984)

[8] W. Götz, N.M. Johnson, C. Chen, H. Liu, C. Kuo, and W. Imler, *Appl. Phys. Lett.* **68**, 3144 (1996)

[9] T. Ogino and M. Aoki, *Jpn J. Appl. Phys.* **19**, 2395 (1980)

[10] E. R. Glaser, T. A. Kennedy, K. Doverspike, L. B. Rowland, D. K. Gaskill, J. A. Freitas, M. A. Khan, D. T. Olson, J. N. Kuznia, and D. K. Wickenden, *Phys. Rev. B* **51**, 13326 (1995)

[11] P. Perlin, T. Suski, H. Teisseyre, M. Leszczynski, I. Grzegory, J. Jun, S. Porowski, P. Boguslawski, J. Bernholc, J. C. Chervin, A. Polian, and T. D. Moustakas, *Phys. Rev. Lett.* **75**, 296 (1995)

[12] E. Calleja, F. J. Sánchez, D. Basak, M. A. Sánchez-Garcia, E. Muñoz, I. Izpura, F. Calle, J. M. G. Tijero, J. L. Sanchez-Rojas, B.

Beaumont, P. Lorenzini, and P. Gibart, *Phys. Rev. B* **55**, 4689 (1996)

[13] S. Nakamura and G. Fasol, "The blue Laser diode" Springer, Heidelberg 1997, chapter 7

[14] F. J. Sánchez, F. Calle, M. A. Sánchez-Garcia, E. Calleja, E. Muños, C. H. Molloy, D. J. Somerford, F. K. Koschnick, K. Michael, and J.-M. Spaeth, pro- ceedings of the European GaN workshop EGW3 in Warsaw, Poland June 1998

[15] S. Nakamura, T. Mukai, M. Senoh, and N. Iwasa, *Jpn. J. Appl. Phys.* **31**, L139 (1992)

[16] S. Nakamura, N. Iwasa, M. Senoh, and T. Mukai, *Jpn. J. Appl. Phys.* **31**, 1258 (1992)

[17] E. Calleja, private communications 1998

[18] F. K. Koschnick, K. Michael, J.-M. Spaeth, B. Beaumont, and P. Gibart, *Phys. Rev. B* **54**, R11042 (1996)

[19] O. H. Han, Hye, Kyung, C. Timken, and E. Oldfield, *J. Chem. Phys.* **89**, 6046 (1988)

[20] J. Neugebauer and Ch. G. Van de Walle, *Phys. Rev. B* **50**, 8067 (1994)

[21] P. Boguslawski, E. L. Briggs, and J. Bernholc, *Phys. Rev. B* **51**, 17255 (1995)

[22] B. Beaumont, S. Haffouz, P. Gibart, M. Leroux, Ph. Lorenzini, *J. CrystalGrowth* in press (1998)

[23] M. Kunzer, U. Kaufmann, K. Maier, J. Schneider, N. Herres, I. Akasaki, and H. Amano, *Mat. Sci. Forum* **143-147**, 87 (1994)

Distribution of Cd^+ paramagnetic centers in CdS under external electric field

N.I.Kashyrina, V.V.Kislyuk, and M.K.Sheinkman

Institute of Semiconductor Physics,
National Academy of Sciences of Ukraine,
prospekt Nauki 45, Kyiv 252650, Ukraine
fax/phone +380 44 265 61 91 email: kislyuk@class.semicond.kiev.ua

The analysis is made for the opportunity of redistributing mobile point defects in a semiconductor affected by the electric field. The voltage is applied in two different ways: i)directly to a sample, ii)to a capacitor plates with a sample between. The model is appropriate also for electric fields of any nature either external or internal including phase interface fields.

INTRODUCTION

An absence of the inversion center in a hexagonal lattice of II-VI crystals, to which CdS belongs, is a cause of the piesoeffect and strong electron- phonon interaction. At the same time, CdS has a complicated spectrum of various local centers. Availability of a variety of investigation methods: photoelectric, optical and methods of radiospectroscopy makes it possible to study a broad range of the phenomena occurring also in other semiconductor materials. CdS can be thereby an appropriate model object to study various processes in semiconductors. A presence of cadmium interstitials (Cd_i) with properties of a paramagnetic center enables to use complex study of the crystal by photoelectric methods and EPR. The EPR study of Cd_i shows that the distribution of donor defects in CdS is substantially non- uniform, the temperature dependence of the EPR line width being attributed to a rather strong exchange interaction between Cd atoms [1]. The interstitial atoms of excess cadmium (Cd_i) are the shallow donors determining n-type conductivity of CdS and of rather high mobility at moderate temperatures $D_{Cd}(500K) \sim 9*10^{-9}$ cm^2/s [2]. At room temperature and below the center is occupied with one or two electrons. The non-compensated crystals contain neutral Cd_i^0 at low temperatures and, thus, do not show any EPR signals, since the main state of the center is a singlet. However, in the compensated crystals some part of the electrons occupies acceptor states, which can gives rise to Cd_i^+ EPR signal. Metastable Cd_i^0 triplet states can arise under the band-band irradiation of the crystal when the conditions appear for the nonequilibrium electrons to be captured both to the singlet and triplet states. EPR spectrum of Cd_i investigated in [1] is, likely, associated with Cd^+, although the authors did not comment a charge of the center but identified it as shallow paramagnetic center of interstitial cadmium. EPR from shallow donors responsible for photochemical reactions in CdS was observed in [3]. The magnitude of the EPR signal decreased as mobile defects were leaving the bulk due to photo-chemical reactions, which allowed to identify the EPR spectrum as associated with mobile defects (presumably Cd_i) [3]. It was proved the EPR spectrum belonged to shallow singly charged centers with S=1/2. The values of g-factors were in consistence with those obtained earlier [4]. Light-induced persistent EPR centers observed in highly compensated CdS was, likely, attributed to a neutral acceptor state [5]. Since the Cd_i concentration defines a non-stoichiometry of CdS with Cd_i tending to form exchange-bounded pairs, it is a mat-

ter of particular consideration to find a correlation between a content of Cd_i ions and anomalous paramagnetic properties of pressure-quenched pure CdS single crystals [6].

This paper considers a possibility of purposeful redistribution of mobile paramagnetic centers under electric field and proposes to apply EPR technique and EPR-tomography to study properties associated with the presence of mobile defects responsible for a conductivity type of a crystal. The mobile point defects in semiconductors give rise to a degradation of the semiconductor devices. The mobile point defects in II-VI compounds are the principal reagent of photochemical reactions found to affect the photosensitivity [7] and luminescence of laser screens [8], to cause formation of conducting channels [9] and changes of properties of metal-semiconductor junction [10, 11]. Since the p-n- or heterojunction is a base of major semiconductor devices, there is always internal electric field to act on the mobile charged defects. It is a problem for manufacturers of Si very large scale integrated circuits (VLSI) and solar cells with a mobility of drifting interstitials to be of substantially high value even at moderate temperatures [12]. The drift of mobile defects can be utilized to redistribute them, decreasing thereby their content within some part of a crystal [13,14].

The paper presents a model which describes the final distribution of the defects after exposure of the field. The model assumes a constant charge state of the drifting ions. The problem was considered for the case of cadmium sulfide.

THEORETICAL BACKGROUND

One - dimensional diffusion-drift equation was used for the electron subsystem in conjunction with Poisson's equation and Boltsman distribution of charged Cd^+ ions (stationary conditions).

With D_n being electron diffusivity, the electron current is expressed as:

$$\vec{i} = -en\mu_n \vec{\nabla}\varphi + eD_n \vec{\nabla} n \,, \tag{1}$$

where φ is the electric field potential, and n is electron concentration.

The mobile donors singly charged are distributed in accordance with Boltsman law:

$$N_{Cd}(x) = N_{Cd}^L \exp\left\{-\frac{e\varphi(x)}{kT}\right\}, \tag{2}$$

where $N_{Cd}(x)$ is concentration of Cd mobile interstitials. With boundary conditions:

$$N_{Cd}(L) = N_{Cd}^L;\ \varphi(L) = 0 \text{ (cathode)};\ \varphi(0) = \varphi_0 \text{ (anode)}.$$

Equations (1) and (2) have to be complemented with Poisson equation which connects potential $\varphi(x)$ with charge density $\rho(x)$:

$$\frac{d^2\varphi}{dx^2} = -\frac{4\pi}{\varepsilon}\rho(x)\,, \tag{3}$$

(4) where $\rho(x) = e(Z_d N_d + Z_a N_a - n(x) + N_{cd}^+(x))$

(hereinafter Z_d=1; Z_a=-1).

Writing electron density as a function of the potential from equation (1) with Boltsman distribution (2) taken into account for the concentration of the mobile Cd ions yields integro-differential equation for the unitless potential $\psi(x) = e\varphi(x)/kT$:

$$(5)\ \frac{\partial^2\psi}{\partial x^2} = \frac{4\pi e^2}{\varepsilon kT}\left\{\frac{in^L}{i_0}e^{\psi}\frac{1}{L}\int_L^x e^{-\psi}dx + n^L e^{\psi} - N_{Cd}^L e^{-\psi} - \Delta N\right\}$$

where $i_0 = en^L D_n / L,\ n^L = n(L)$.

The diffusivity D_n and mobility μ_n are connected by Einstein's equation.

Equation (5) can be easily rewritten in terms of the electric field:

$$\frac{\partial^2 E}{\partial x^2} + \frac{e}{kT}E\frac{\partial E}{\partial x} - \frac{4\pi e^2}{\varepsilon kT}\times \tag{6}$$

$$(2N_{Cd}^L e^{-\psi} + \Delta N)E + \frac{4\pi i}{\varepsilon kT}\frac{e}{kT} = 0$$

where $\Delta N = N_d - N_a$.

At $N_{Cd}^{L} = 0$eq.(6) transforms into the well-known equation for the field distribution within a space charge region [15]. The presence of the mobile donors actually expands the space charge region over Debye's length determined as:

$$L_D = \left(\frac{\varepsilon kT}{4\pi e^2 \sum_k n_k Z_k^2} \right)^{1/2}$$

where Z_k is a charge of k_{th} component, to the whole length of the crystal.

Equation (6) can be solved by the successive approximation method. As a zero approximation can be taken the $N_{Cd}(x)$ distribution calculated in quasi-neutrality approach. Substituting zero approximation $N_{Cd}(x)$ into eq. (6) we can analyze the current-voltage dependence in first approximation. A convergence of the method is determined by L_D/L ratio.

RESULTS AND DISCUSSIONS

The right side of eq. (6) is zero in quasi-neutrality approach, and thus we get the potential $\psi(x)$ as an implicit function in the expression:

$$\frac{x}{L} = 1 - \frac{F(\psi)}{F(\psi_0)}, \quad (7)$$

where $$F(\psi) = e^{-\psi} - \frac{\Delta N}{2N_{Cd}^{L}}\psi - 1$$

According as the charge of the "background" is positive or negative (corresponds to sign of ΔN (7) tends to behave in properly different ways. While for $\Delta N > 0$ there is a continuous solution of eq. (7) (At $\Delta N = 0$ it becomes an expression used in the theory of binary electrolytes [16]), this is not the case when the "background" is negatively charged. The solution in such a case has a break, which indicates an invalidity of the electroneutrality approach. At any rate, both cases have similar solutions for $\psi_0 \le 3$ (Fig.1). A result obtained for the system with immovable positively charged background is the most attractive since these conditions allows to extend zone with low Cd^+ content (fig.2, curves 1, 2, 3 correspond to i/i_0= 3, 5, 10 respectively).

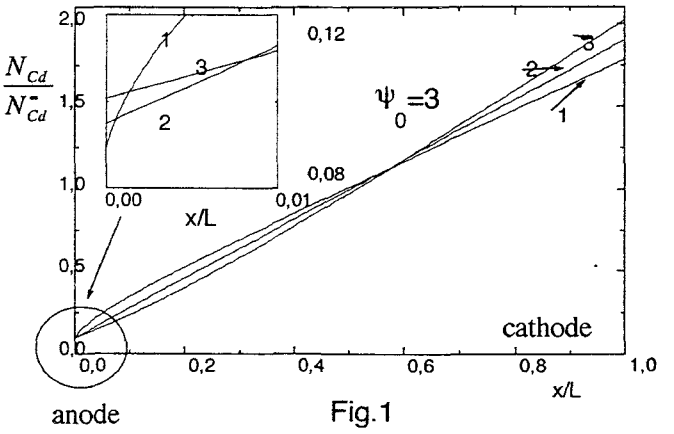

Fig.1

Figure 1. Redistribution of Cd^+ concentration for a system which includes: (1) - three components (electrons + Cd_i + immovable acceptors; N_a/N^L_{Cd+}=0.1); (2) - two components; (3) - three components (electrons + Cd_i + immovable donors; N_d/N^L_{Cd+}=0.1).

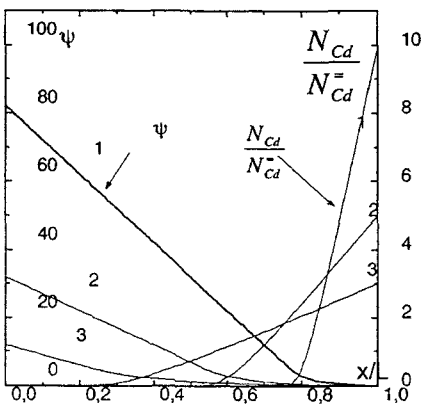

Fig. 2

Figure 2. Redistribution of Cd^+ concentration and voltage (in terms of unitless potential $\psi(x)$) at the case of the positive "background" for various values of current: 1 - i/i_0=3; 2 - i/i_0=5; 3 - i/i_0=10.

When i/i_0 value is rather low the first term within the parenthesis in eq. (5) becomes:

$$\frac{\partial^2 \psi}{\partial x^2} = \frac{4\pi e^2}{\varepsilon kT} \times \left\{ n^L e^{\psi} - N_{Cd}^{L} e^{-\psi} - \Delta N \right\} \quad (8)$$

which describes the electric field between the plates of a capacitor. Eq. (8) with $\Delta N = 0$ and boundary conditions: $\psi(0) = \psi_0/2; \psi(L) = -\psi_0/2$ transforms into

Poisson-Boltsman equation:

$$\frac{\partial^2\psi}{\partial x^2} = \frac{4\pi e^2}{\varepsilon kT} n^0 \left\{ e^{\psi} - e^{-\psi} \right\} \tag{9}$$

which is solved analytically at boundary conditions taken as: x=L; $\psi(x) = 0$ and the other usually determines a value of the field at x=0. The value of the field within a sample at $i/i_0 \sim 0$ is negligible at x far from edges of the crystal (fig.3).

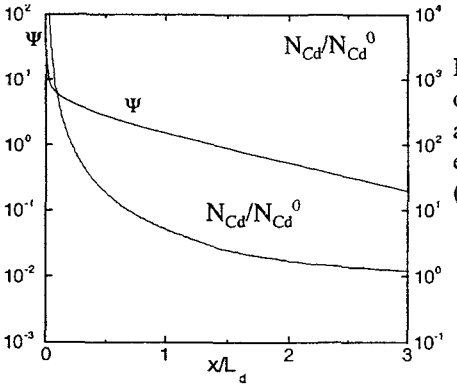

Figure 3. Distribution of ion concentration and potential of the electric field at $i/i_0 \sim 0$ (capacitor).

The potential distribution within the space charge region (SCR) is determined by the integral:

$$\frac{x}{L_D} = \int_{\psi_1}^{\psi_0/2} \frac{d\psi}{\sqrt{e^{\psi} + e^{-\psi} - 2}} \tag{10}$$

A surface charge confined by the external field within a thin ($\sim L_D$ thickness) within surface layer is calculated by

$$Q = eL_D n_0 \int_{\psi}^{\psi_0/2} \frac{(e^{\psi} - e^{-\psi})d\psi}{\sqrt{e^{\psi} + e^{-\psi} - 2}} \tag{11}$$

where e and n_0 are the electron charge and concentration in the bulk where it equals the donor concentration N_{Cd}^0 and can be obtained from the normality condition:

$$N_{Cd}^{=} L = N_{Cd}^0 \int_0^L e^{\psi(x)} dx \tag{12}$$

The right - hand side of eq. (12) contains the total quantity of Cd^+ ions redistributing in the sample. The term from the left side N_{Cd} L determines a number of the ions before the electric field was applied with the uniform initial distribution of the ions taken into account.

Figure 4 shows that at the potential $\psi_0 = 60 - 80$ contents of the mobile defects decreases in 3-4 orders of magnitude. (for L=1 cm). Whereby Cd ions are confined within a thin layer ~ $10L_D$ (L_D - Debye's length $L_D = 10^{-5}$ cm for $N_{Cd} = 10^{15}$ cm^{-3}, T=300K).

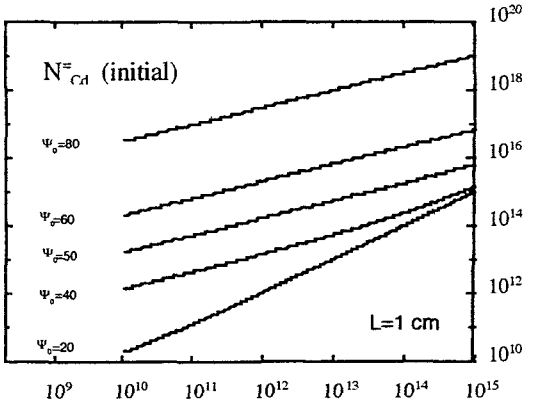

Fig.4 N^0_{Cd} (final)

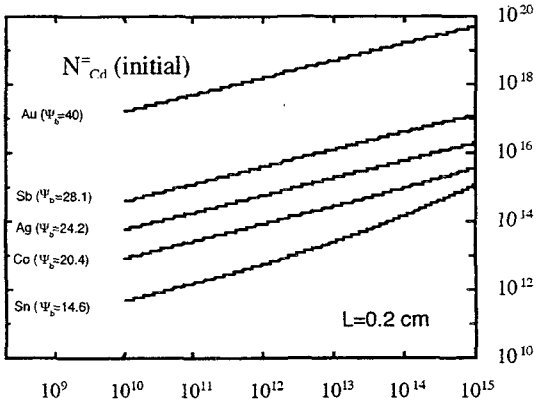

Fig.5 N^0_{Cd} (final)

Figures 4 and 5. Diagrams to determine the anticipated value of a final (stationary) concentration of mobile Cd ions in the bulk (N^0_{Cd}) for a certain value of the initial concentration of uniform distribution ($N^{=}_{Cd}$) at various magnitudes of applied potential ψ_0 (**Fig.4** for the case of external electric field) or contact barrier potential ψ_b (**Fig.5** for the case of Schottky barrier potential formed by the deposition of metals Sn, Co, Ag, Sb, Au [17]). The potential values are presented in kT/e units.

Obviously, Cd^+ redistribution caused by external electric field (fig.4) can be formed by electric field of an-

other nature. The capacity of space charge layer near the edge of the crystal is associated with potential $\psi_0/2$ This potential may originate from a phase interface. Fig.5 demonstrates the values of the bulk concentration of mobile Cd which can be reached by the action of the electric field on the metal - CdS interface for various metals. The values of contact barriers ψ_b (in kT/e units) were taken from [17]. ψ_b (in terms used above) corresponds to $\psi_0/2$ in formula (10) and on fig.4. Cd^+ redistribution presented on fig.5 is calculated for crystals of length L=0.2 cm at the assumption that one face of a crystal is coated with a metal deposited thereon.

CONCLUSIONS

The possibility is considered to clean out mobile charged defects from the bulk of a crystal by means of electric field. The calculations concern only a stationary limit which can be taken as a boundary condition for a transient problem at $t \to \infty$. Hence, our analysis demonstrates the potentialities (determined by absolute minimum of the system energy) which could be realized by the action of the electric field. The most appropriate conditions for the "cleaning" are those with $\Delta N > 0$, while otherwise at $\Delta N < 0$. The transition from $\Delta N > 0$ to $\Delta N < 0$ could be reached using band-to-band irradiation of the crystal. Experimentally this phenomena was observed in [15], where the crystal irradiated with absorbed light was cleaned of mobile defects over the 1/4 of the crystal length.

Schottky barrier field was considered to be effective to decrease content of mobile defects. The calculations were presented for various contacting metals.

ACKNOWLEDGMENT

The authors wish to thank prof. N.E.Korsunskaya and prof. N.B.Lukyanchikova for fruitful discussions and useful remarks.

REFERENCES

[1]V.Ya.Bratus', I.M.Zaritskiy, G.S.Pekar et al.: FTP (Fiz. Tekhn. Poluprov.- Physics and Technique of Semiconductors) 14, 1339-1342 (1980)

[2]Pronichkin V.D., Polishchuk V.E., Ignatov A.V.: Surface 1, 142 -145 (1987)

[3]Baran N.P., Dzhumayev B.R., Korsunskaya N.E., Markevich I.V., Khomenkova L.Yu., Shulga Ye.P.: FTT 38, 1735-1741 (1996)

[4]Toyotomi J.: J.Phys.Soc. of Japan 31, 511-523 (1971)

[5]Dong M., Honig A., Light-induced persistent EPR centers in highly compensated CdS, Thes. of American Physical Society Meeting, St. Louis, Missouri, USA, 20-24 March 1996

[6]MacCrone R.K., Homan C.G.: Sol. State Com., 35, 615-618 (1980)

[7]Sheinkman M.K., Korsunskaya N.E.: Photochemical reactions in II-VI semiconductors in col. pap. Physics of II-VI compounds ed. by Georgobiany A.N.and Sheinkman M.K., p. 109, Moscow, Nauka 1986 (in Russian)

[8]Akimov I.V., Korostelin V.I., Akimova I.V., Kozlovskiy V.I., Korostelin Yu.V.: Proc. of Lebedev Inst., 177, 142- (1987)

[9]Drozdova I.A., Embergenov B., Korsunskaya N.E., Markevich I.V., Singaevski A.F.: FTP 29, 536-542 (1995)

[10]Oginskas A., Bertulis K., Chesnis A., Shiktorov N.: Lit. Fiz. Sbornik (Lithuanian col. Pap.) 21, 37-43 (1981)

[11]Drozdova I.A., Embergenov B., Korsunskaya N.E., Markevich I.V.: FTP, 27, 674-675 (1993)

[12]Heiser T., Mesli A.: Appl.Phys., A57, 325-328 (1993)

[13]Korsunskaya N.E.,.Markevich I.V, Torchinskaya T.V., Sheinkman M.K: FTP, 13, 435-437 (1979)

[14]Kislyuk V.V., Korsunskaya N.E., Markevich I.V., Pekar G.S., Sheinkman M.K.: FTP, 30, 1884-1888 (1996)

[15]Bonch-Bruyevich V.L., Kalashnikov F.D., Physics of Semiconductors, Nauka, Moscow, 1977.

[16]Newman J.S., Electro-chemical Systems, Prentice-Hall Inc., Englewood Cliffs, NJ, 1973

[17]Forsyth N.M., Dharmadasa I.M., Sobiesierski Z., Williams R.H.: Semicond. Sci. & Technol., 4, 57-59 (1989)

Superoxide Scavenger Copper(II) Complexes having Bis(Hydrazino-Triazine) Ligands: an EPR and MM$^+$ Study

C. G. Palivan, C. E. Darmon, St. Thomas[1]

University of Bucharest, Faculty of Physics, Department of Atomic and Nuclear Physics, Bucharest-Magurele, P.O. Box MG-11, Romania

[1]University Polytechnica, Faculty of Chemistry, Department. of Dyes, Calea Victoriei 149, Bucharest, Romania

Abstract

EPR spectrometry and molecular mechanics force-field calculus were used to characterize the coordination around the metal ions in a series of four superoxide scavenger copper complexes having bis(hydrazino-triazine) ligands. The distorted 2N2O square planar arrangement around copper as well as the presence of 4N coordination is proposed as an explanation for the difference between their activity and those described in a previous study.

Introduction

Superoxide dismutase (SOD) and related copper complexes have been proposed as medicinal agents to decrease the concentration of superoxide free radical anion $O_2^{\bullet-}$ during pathological phenomena [1]. The high molecular weight of the natural proteins considerably limits their membrane permeability and for this reason low molecular weight copper complexes were synthesised as potential anti-inflammatory and anti-viral drugs [2]. Furthermore, toxicological studies revealed that anti-inflammatory copper complexes are less toxic than inorganic forms of copper.

Previous studies have shown that EPR spectrometry and molecular dynamics calculations [3,4] can give insight into the structure of the first order coordination sphere around the metal ion in a class of asymmetric triazine complexes, having anti-viral activity. In this study we extend the characterisation of the structure of the Cu(II)-complexes to a group of four complexes having hydrazino-triazine ligands, with possible biological activity.

Experimental

Complexes I, II, III and IV are the bis complexes of the hydrazino-triazine ligands presented in Fig. 1, respectively. The copper complexes were made following the general method described in [5]. The complexes were analysed for C, H (elemental analysis) and Cu (atomic absorption spectrometry) and their IR spectra were recorded on a C. Zeiss (Jena) Model M80 spectrometer, the analytical results for the various preparations being listed in [6].

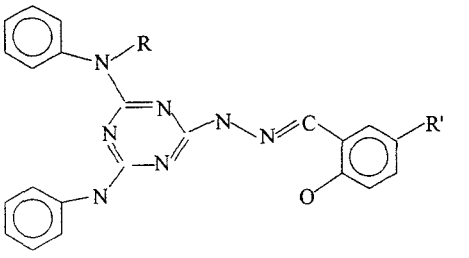

Ligand	I	II	III	IV
R	H	CH_3	H	CH_3
R'	H	H	NO_2	NO_2

Fig. 1 Hydrazino-triazine used as ligands of copper complexes

In vitro assessments of superoxide dismutase activity were done by measuring the concentration of $O_2^{\bullet-}$ radicals in solutions using the photometric method of [7].

Samples for EPR measurements were prepared as follows: a) powder without any further treatment; b) saturated fluid solutions prepared by heating an excess of the complex in DMF/methanol (7:1), at 50° for 5 min, followed by filtration to remove any undissolved solid.

EPR spectra at ambient temperature and 77K were obtained using a Jeol JES-Me 3X spectrometer with 100kHz field modulation,

operating at 9.1 GHz. Optimization of spectral resolution was achived by making multiple accumulations and using fast Fourier transformation with Gaussian profile for subsequent noise reduction.

The simulation of the spectra in order to estimate the EPR parameters were done using a home made iterative program (Minuit-Simplex) based on a second perturbation algorithm with co-axial **g** and hyperfine tensors. The lineshapes for the frozen solutions were Gaussian with different widths according to the overall shape of the signal, while for solution simulations, a Lorentzian lineshape was used. All the simulations consider the copper isotopes in their natural abundance.

Theoretical structures for the copper complexes of the various ligands were calculated using the molecular mechanics force-field algorithm MM^{+} [8].

Results and discussion

The biological activities of the bis-complexes were higher than those of the uncomplexed ligands, but they were less active than the complexes previously analysed [4]. The superoxide scavenging activities of the various complexes were in order: CI>CIII>CII>CIV, altough the differences between them are small.

The analysis of the polycrystalline EPR spectra at room temperature shows that the synthetic process yields copper complexes in two forms: monomeric Cu(II) species for all the complexes and a very small concentration of dimeric species, for Complexes I, III and IV.

The powder EPR spectra of the various complexes show differences in overall shape as can be seen in Fig. 2. In all the cases the spectra appear to be a mixture of components and their simulations, derived from the EPR parameters in Table 1, are shown in Fig. 2.

The fluid solutions of fast-tumbling copper complexes are isotropic in character, but there are extensive line-width variations, common with copper complexes due to the insufficiently rapid molecular motion to completely average the anisotropic interactions.

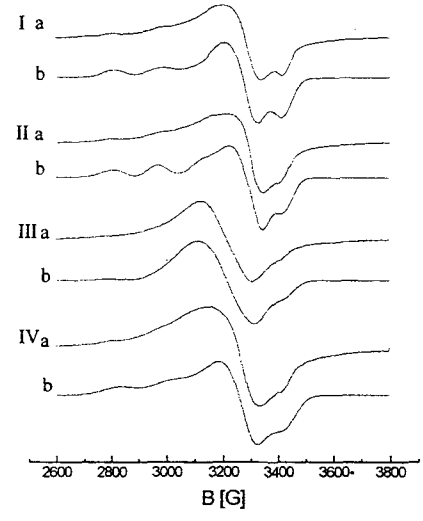

Fig. 2 EPR powder spectra at room temperature for Complexes I, II, III and IV: a) experimental, b) simulated with the EPR parameters in Table 1

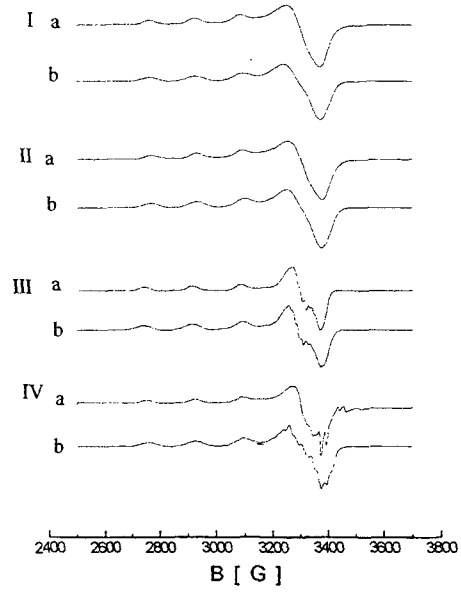

Fig. 3 EPR spectra at 77°K of DMF/methanol solutions of Cu(II)- complexes: a) experimental; b) simulated using the EPR parameters in Table 1

The spectra appear as simple components, but their poor resolution does not give insight into the structure.

The different features of these complexes are clearly revealed by the EPR spectra recorded in frozen solutions (Fig. 3).

Table 1 EPR parameters of Complexes I, II, III IV and I*[4] (* = dimers, p = powder, s = solution)

Comp	g			A [Mhz]		
	g_{xx}	g_{yy}	g_{zz}	A_{xx}	A_{yy}	A_{zz}
I*-p						
A	2.060	2.068	2.205	30.1	70.0	555.0
B	2.082	2.087	2.257	53.0	47.0	427.0
I - s	2.054	2.077	2.258	50.2	70.0	508.0
II - p						
A	2.056	2.062	2.194	42.0	75.0	570.0
B	2.075	2.086	2.235	50.0	65.0	445.0
II - s	2.045	2.081	2.256	41.0	65.0	512.0
III*-p						
A	2.065	2.104	2.197		-	
B	2.060	2.063	2.215	21.0	45.0	580.0
III-s						
A	2.057	2.070	2.265	25.0	30.0	542.0
B	2.065	2.072	2.251	35.0	35.0	550.0
IV*- p	2.088	2.095	2.245	50.1	65.2	435.1
	2.071	2.075	2.192	45.4	30.1	565.0
IV-s						
A	2.056	2.066	2.260	75.7	85.8	530.5
B	2.054	2.056	2.253	21.1	26.4	501.2
I**-s						
A	2.031	2.106	2.234	71.0	88.4	537.4

The frozen solutions spectra of Complexes I and II can be simulated in a consistent way as single components whereas at least two species of comparable intensities are present for Complexes III and IV. This suggests that the mixture of components observed in powder for Complexes I and II have similar anisotropic parameters and are probably closely related.

The **g** and hyperfine splittings obtained from the best fit of the spectra are presented in Table 1 along with those of the most active complex from the previous study [4].

The magnetic parameters obtained for these complexes in the $g_{//}$ region are in agreement with values of $g_{zz} > g_{xx,yy} > 2.040$ suggesting a $d_{x^2-y^2}$ ground state, characteristic for square planar, square-base pyramidal or octahedral first sphere arrangement around the metal ion [9]. In the case of these complexes we propose a distorted square-planar arrangement around the copper ion. Even though the first coordination sphere around the metal has the same type of chromophors, the EPR parameters show a slight variation which can be associated with a specific modification of the ligand structure. The change of R' from H to NO_2 increases slightly the A_{zz} value, as it can be seen for Complexes II and IV, for example.

For this class of complexes, the f factor (g_{zz}/A_{zz}) [10] can be used as a distortion parameter and its values show that the introduction of NO_2 changes slightly the distortion of the geometrical arrangement around copper compared with that of the complex without NO_2 (see Table 2).

Table 2 Superhyperfine ^{14}N coupling and f factor values of Complexes

Comp.	f [cm]	A_N [MHz]	Coord.
I	133.3	45	2N
II	132.1	-	-
III	125.3	45	4N
	122.6	47	2N
IV	127.8	48	2N
	134.8	54	4N
I*[4]	124.6	45	2N

The various features of these complexes can be seen in the 2nd derivative recordings, especially in the perpendicular region. As usual, in the perpendicular region there are superposed the perpendicular components of copper, the forbidden transitions depending on the copper

quadrupole interaction which varies with the ligation, and the ^{14}N hyperfine couplings. Furthermore, the perpendicular region is dominated under a wide range of conditions by so-called overshoot lines arising from an interplay of g and A anisotropies and finally the presence of ^{65}Cu isotope will change the intensity and the position of the hole pattern. For all these reasons, the perpendicular region of the spectrum is always difficult to simulate without resolution of the superhyperfine structure in the $g_{//}$ region.

The analysis of the superhyperfine coupling to ^{14}N atoms shows the presence of two types of copper environment: 2N2O for Complexes I, III and IV and 4N for Complexes III and IV; the hyperfine constants are presented in Table 2.

It seems that the NO_2 presence in the ligand changes not only the geometry around the metal ion, but determines an additional type of complexation, too. Despite the EPR variation in parameters, the fact that the arrangement of the copper ion does not change dramatically (as it can be seen by analysing the values of the f factor, [10]) can explain why these complexes have no great differences in their biological activity.

Table 3 Molecular mechanics force-field calculations of optimized geometrical arrangements of copper(II) complexes (tth = tetrahedral; sq. = square; oth. = octahedral, pyr = pyramidal)

Comp	Coord.	Structure	Energy [kcal/mol]
I a	2N2O	distorted tth	35.26
b		"	48.27
c		distorted sq. pyr.	68.36
II a	2N2O	distorted tth	81,30
b		distorted sq. pyr.	87.94
III a	2N2O	distorted tth	41.42
b	4N2O	distorted oth	165.20
IV a	2N2O	distorted tth	97.21
b	4N2O	distorted oth	232.41
I* a	2N2O	square planar	213.0

The biological activity is smaller for the complexes containing NO_2, associated with the slight modification around the copper ion and the presence of 4N coordination.

The MM^+ calculations of possible geometrical arrangements for the various complexes show that more than one type of structure is possible (Table 3) with 2N2O environment around the copper (all complexes), whereas III and IV could also exist with 4N2O coordination.

All the structures present tetrahedral or tetragonal distortions with respect to the square planar geometry which characterizes the most active complex previously analysed I* [4] and we suppose that the geometrical arrangement around copper as well as the presence of 4N coordination type can explain the difference in biological activity of these complexes compared with the ones previously analysed.

Conclusion

EPR spectroscopy and MM^+ calculation were used to distinguish different types of coordination environment for copper in a class of bis[hydrazino-triazine] Cu(II) complexes with a range of SOD activity in order to understand why their biological activity is smaller than the previous most active complex.

The EPR spectrometry can be used as a specific tool to gain insight into the effect of structural modifications of copper coordination between the complexes of the same class.

Acknowledgements

We thank Dr. A. Zuivertz for providing data on the superoxide dismutase activities of these complexes.

Bibliography

1. J.R.J. Sorenson, Comprehensive Therapy, 11(4), 49, 1985

2. L. Bergendi, J. Kratsmar-Smgrovic, Z. Durakova, I.Zitnanova, Free. Rad. Res. Commun,

12-13, 195, 1991
3. A. Popescu, J. Jucu, E. Tomas, A. Zuivertz, C. Cristescu, St. Thomas - Rev. Roum. Medicine Virol. 43, 129, 1992
4. B.A. Goodman, C.G. Palivan, C. Cristescu - Polyhedron, 14 (17-18), 2523, 1995
5. C. Cristescu, St. Thomas, F. Czobor, Rev. Roum. Chem., 1998, in press
6. St. Thomas, private communication
7. E. Thomas, A. Popescu, A. Titire, N. Cajal, C. Cristescu, St. Thomas, Rev. Roum. Medicine. Virol., 40, 305, 1989
8. N.L. Allinger, J. Am. Chem. Soc. 99, 8127, 1977
9. B.J. Hathaway, D.E. Billing, Coord. Chem. Rev., 5, 143, 1970
10. U. Sakaguchi, A.W. Addison, J. Chem. Soc. Dalton Trans, 600, 1979

Antiphase Domain Structure as Studied by EPR

W.Zapart and M.B.Zapart
Institute of Physics, Technical University, 42-200 Czestochowa, Poland

1.Introduction

The symmetry reduction occurring at a structural phase transition results in a formation of domain structure. In proper or pseudoproper ferroelastics this structure is based on orientational domains as the result of loosing the elements of point group symmetry. In improper ferroelastics both orientational and antiphase domains exist; the latter are due to a lowering of the translational symmetry of the crystal (a doubling of the unit cell size). The antiphase boundaries in improper ferroelastics separate two domains with the same spontaneous strain and can be treated as resulting by introduction (or removing) an additional half a unit cell. This should be an origin of additional strain fields in the crystal structure therefore one could expect that in order to minimize this strain the antiphase domain wall should be a transient region of rather large dimension [1].

The antiphase boundaries (APB) are usually assumed to have a linear structure which is represented by the kink-solution :

$$Q(x)=Q_o \tanh(k\,x) \qquad (1)$$

where k^{-1} is the measure of domain wall thickness , the x-axis is normal to the APB plane and Q_o is the value of order parameter inside the two domains. Fig. 1 depicts the order parameter profile for the antiphase boundary separating two regions with structures mutually shifted by a translation lost at transition .

If the amount of the relative shift of the atomic position in two opposite domains is as small as the amplitude of thermal vibration [2], these domains are expected to be connected without any special layer (Fig.1b). In the case when this relative atomic shift is far larger the thick domain wall is to be expected (Fig.1c).

Of particular interest are the studies of the domain walls by optical techniques or by electron microscopy. However, in some ferroelastic phases a dense network of periodic domain walls can provide their observation by electron paramagnetic resonance.

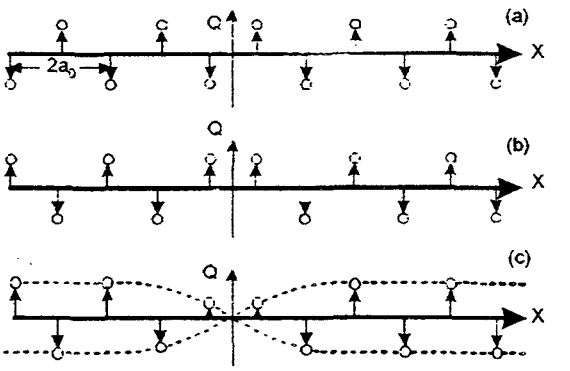

Fig.1 Structure and schematic order parameter profile for the APB: a) single domain, b) discontinuous APB , c) continuous APB

Our earlier papers [3-5] reported the changes in the EPR line shape produced by lattice distortions associated with the ferroelastic domain walls.

It is the purpose of this paper to evaluate the effects of the spatial variation of order parameter on the EPR line shape in systems exhibiting a periodic antiphase domain structure. It is shown that in such a case paramagnetic centers lying in the domains as well in the intermediate regions-domain walls can contribute to the overall EPR line shape. This model is applied to the EPR data available in the literature for crystals belonging to a family of fluosilicates in which the existence of dense antiphase domain structure has been reported [6].

2. EPR studies of phase transitions and twinning

Electron paramagnetic resonance is a powerful tool in investigations of structural phase transitions in crystals. The usefulness of this method arises from the fact that the magnetic resonance field is a function of the order parameter of the transition. The temperature evolution of the order parameter is usually observed by characteristic changes in the spin Hamiltonian parameters. The radiospectroscopic methods applied to phase transition studies were developed firstly for ferroics described by a spatially uniform order parameter. In the last two decades they have been successfully applied to study the incommensurate systems described by spatially non-uniform order parameter [7] .

The crystal symmetry reduction occurring at the transition is also detected by EPR. The unit cell multiplication occurring at improper phase transitions is observed through the splitting of the resonance lines . The additional line splitting could be present due to a dividing the crystal into the orientational domains [8]. The antiphase domain structure does not cause any splitting of the EPR lines thus it „is seen" by the EPR as one orientational domain.

In multi-domain crystals the observed EPR lines are usually attributed to paramagnetic centers lying in the domains. The above is true on the assumption that a volume of the domains is much greater than the effective volume occupied by the domain walls. In the case when the effective volume of the domain walls becomes comparable with that of domains one can expect to find in the EPR spectrum the contributions from the paramagnetic centers lying in the domain walls [3].

Such a situation can be realized in the systems described by the non-uniform order parameter in which a periodic microdomain structure occurs. Fig.2 depicts the structure of domain walls and the expected EPR line shape for different percentage contribution of the domain walls with respect to the crystal volume.

When microdomain structure is characterized by a high density of domain walls or by a thickness of domain wall comparable with the domain size the EPR spectrum can be affected through a significant broadening of the resonance lines or it can take an incommensurate-like form (as in Fig.2c) .

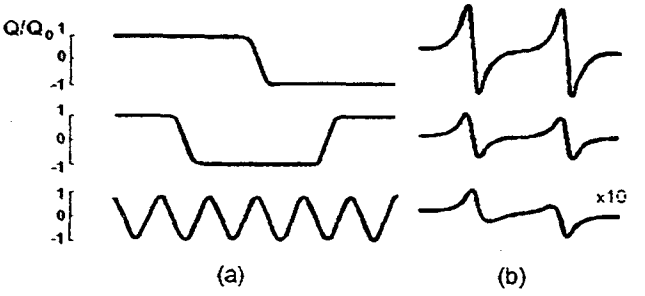

Fig.2 Different percentage contribution of domain wall volume with respect to the crystal volume (a) domain wall structure , (b) simulated EPR line shape (a linear case, B_1 = 12 mT). The upper curve corresponds to 4% ($kx \approx 24$), the central curve - 8% ($kx \approx 12$) and the bottom curve - 50% ($kx \approx 2$) .

Such an experimental situation occurs in the $KSc(MoO_4)_2$ crystal where by means of TEM a regular ferroelastic microdomain structure with the high density of domain walls has been found in the vicinity of phase transition temperature T_3 =181 K [5] . The EPR line shape of Cr^{3+} complexes observed in this temperature interval is similar to that observed in incommensurately modulated systems. Also an unusual shape of the resonance lines for Cr^{3+} in $Pb_3(PO_4)_2$ [4] observed in the temperature range 160-180 ^{0}C was explained as the effect of ferroelastic microdomain structure with the domain wall thickness greater than 6 nm .

So far the influence of periodic antiphase domain structure on the EPR spectra has been not discussed in the literature.

3. EPR line shape analysis

According to equation (1) the order parameter value inside the domain wall is less than that in the domain. So if one assumes that the splitting of the resonance lines corresponds to the maximal value of the order parameter, the EPR lines origi-

nating from the centers lying in the domain wall should be in between of these split lines. The basic assumption of the presented model , similar to the procedure developed for incommensurately modulated phases [7] is that the resonance magnetic field can be expanded into the power series of the order parameter yielding :

$$B = B_1 \tanh(kx) + B_2 \tanh^2(kx) + \ldots \qquad (2)$$

The coefficients B_1 , B_2 , .. depend on the symmetry of the paramagnetic center site and the direction of the external magnetic field with respect to the symmetry elements of the crystal lattice.

The resonance field distribution function f(B) that determines the EPR line shape is given by :

$$f(B) = 2\pi / (dB/dx) \qquad (3)$$

The overall EPR line shape F(B) is given by convoluting the resonance field distribution function f(B) with the line shape function $L(B-B_c)$ of a single line:

$$F(B) = \int L(B - B_c)\, f(B_c)\, dB_c \qquad (4)$$

The singularities in the line shape are determined by the zeros of the derivative dB/dx in eq.3. Let us consider some special cases :

a) when only linear term in eq.2 is dominant ($B_1 \neq 0, B_2 = 0$)

Then eq.3 becomes:

$$f(B) = \left(2\pi/k\right)\frac{\cosh^2(kx)}{B_1} = \frac{2\pi/k}{\left[B_1 - \dfrac{(B - B_0)^2}{B_1}\right]} \qquad (5)$$

We find that the function f(B) has the characteristic edge singularities at two values of the magnetic field ,

$$B_{\pm} = B_0 \pm B_1 \qquad (6)$$

Fig. 3a shows a plot of the above function against $(B-B_0)$.

b) when the quadratic term is dominant, ($B_1 = 0$ and $B_2 \neq 0$) .

Eq.3 becomes :

$$f(B) = \frac{2\pi \cosh^2 kx}{B_2 k \tanh \Phi(x)} =$$

$$= \frac{2\pi/k}{2B_2\sqrt{\dfrac{(B - B_0)}{B_2}\left(1 - \dfrac{(B - B_0)}{B_2}\right)}} \qquad (7)$$

Fig. 3c presents a plot of the f(B) in the quadratic case . It is worth noting that now f(B) is asymmetric in shape. There are two singularities at :

$$B = B_0 \quad \text{and} \quad B = B_0 + B_2 \qquad (8)$$

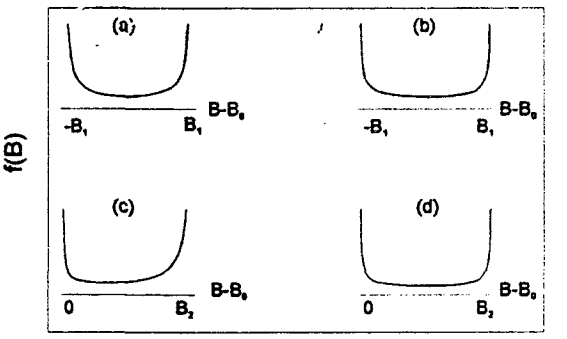

Fig.3 Magnetic resonance field distribution in linear case (upper raw) and quadratic case (lower raw): (a) and (c) correspond to the eq. 5 and 7, respectively ; for comparison (b) and (d) depict f(B) in incommensurately modulated systems

The position of one singularity represents a continuation of the para-phase line at $B=B_0$.

For the comparison , the distribution function f(B) for incommensurately modulated systems is shown in Fig. 3b and 3d for linear and quadratic cases, respectively.

4. Experimental example.

$Mg(SiF_6).6H_2O$ crystallizes in the high temperature phase in the trigonal system . At the temperature T_1 =363 K (90 °C) a second order phase transition occurs in this crystal and at T_2=298K (25 °C) a ferroelastic phase transition of first order to the monoclinic phase is observed. In the intermediate phase, below trigonal and above

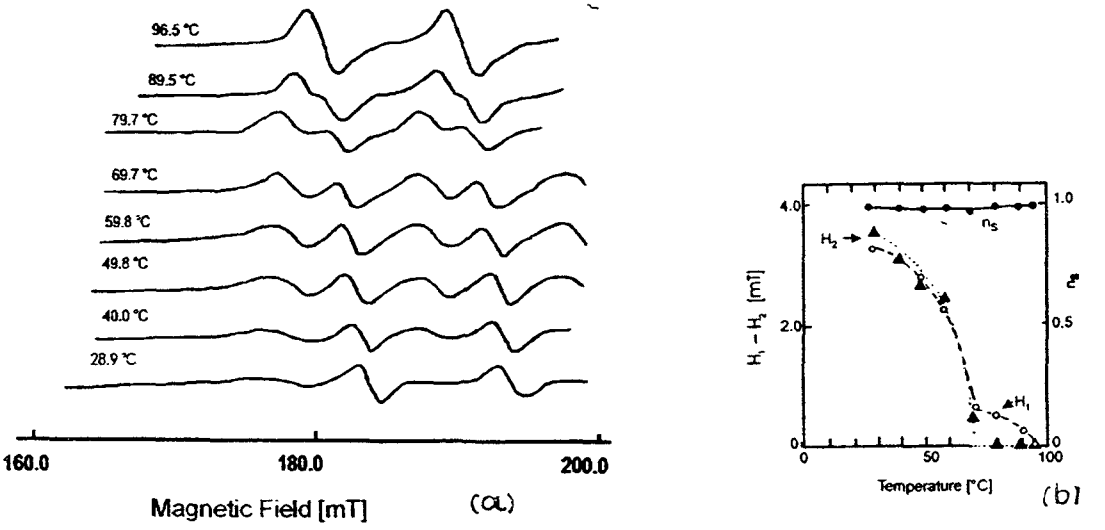

Fig.4 Temperature changes : (a) in the low-field part of the EPR in $Mg[H_2O]_6\ SiF_6$: Mn^{2+} crystal, (b) in the modulation amplitudes, H_1 and H_2 and the soliton density [ref. 10]. Magnetic field is parallel to the c-axis.

monoclinic ones, a periodic antiphase domain structure was reported [6] by X-ray studies, with the period equal to seven unit cells. The EPR studies [9,10] revealed that in this temperature region the resonance lines are unusually broadened and their positions are limited by two edge singularities. Hence the conception about the existence of the incommensurate phase was postulated from the EPR studies. Since neither rentgenographic nor neutronographic methods did reveal satellite reflections in the incommensurate positions our attempt is to develop an alternative approach to the interpretation of the EPR line shape in this crystal in the framework of regular antiphase domain structure

Figure 4a presents the temperature evolution of the EPR spectrum of Mn^{2+} in $Mg(SiF_6).6H_2O$ reported in [10]. The spectrum obtained for the

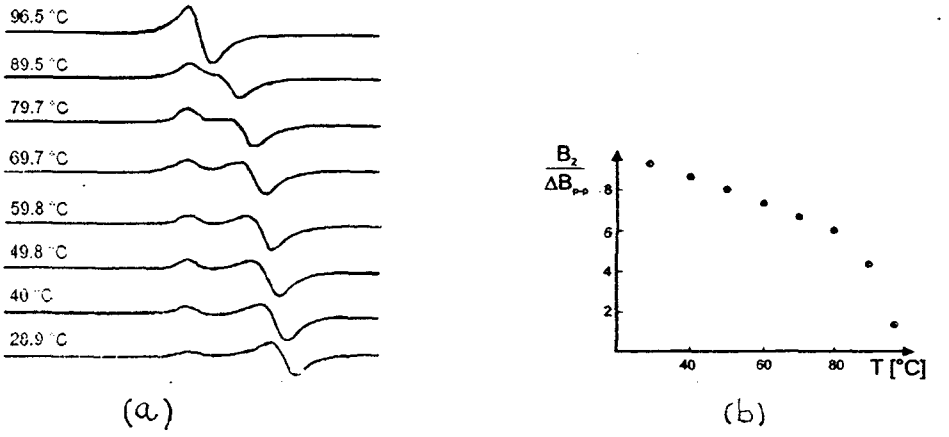

Fig.5 (a) Computer generated EPR spectra for the case where the term quadratic in Q is dominant. The parameter d=kx takes values from 2 at 96.5 C to 4 at 28.9 C. b) Temperature variation of the parameter B_2 .

magnetic field parallel to the threefold axis of the crystal shows that the splitting of peaks begins at 96 °C. The changes of the line shape with the temperature allow the authors to find a temperature evolution of the parameters H_1 and H_2 describing the expansion of the magnetic resonance field in powers of the incommensurate displacement wave (Fig.4b). The left part of the EPR spectrum was taken into consideration in our analysis.

Using eq.4 we simulated the EPR spectrum for the quadratic case since the parameter B_1 in the eq.2 should be equal to zero for the above mentioned orientation of the crystal . Fig.5a presents the simulated line shapes where the fitting parameters are B_2 and the domain extension d=kx. Fig.5 b shows the temperature changes of the parameter B_2 obtained from the comparison of the simulated and experimental spectra. One can conclude that on lowering the temperature the domain volume increases with respect to the volume occupied by the domain walls .

5. Concluding remarks.

The $MgSiF_6.(6H_2O)$ crystal seems to be unique in which the EPR spectrum in the phase characterized by the periodic antiphase domain structure was obtained so it was chosen for checking the theoretical predictions of the presented above model of the EPR line shape. It has been shown that the observed incommensurate-like EPR spectrum in the manganese fluosilicate can be explained in the framework of regular antiphase domain structure taking into consideration only the quadratic model. In the papers assuming the existence of the incommensurate phase in the $Mg(SiF_6).6H_2O$ crystal the authors described the EPR spectra by two linear and quadratic terms, despite the fact that linear coefficients are not symmetry allowed for the magnetic field orientation chosen by them.

Thus the presented here approach is consistent as well with the symmetry requirements as with papers suggesting the antiphase domain structure in the intermediate phase in this crystal.

References

[1] I.Rychetsky, W.Schranz, J.Phys.:Condens.Matter **5** , 1455 (1993)
[2] M.Takagi, S. Suzuki, J. Phys.Soc. Japan **63** , 1580 (1994)
[3] M.B.Zapart , Ferroelectrics **141** , 67 (1993)
[4] M.B.Zapart, W.Zapart, M.S.Jang, S.Y.Jeong, Ferroelectrics **172** , 437 (1995)
[5] M.B. Zapart , E. Snoeck, P.Saint-Gregoire, Ferroelectrics, **191**, 179 (1997)
[6] G.Chevrier, G. Jehanno, Acta Cryst. **A35**, 912 (1979)
[7]. R.Blinc , P.Prelovsek, V. Rutar, J.Seliger, S.Zumer in „Incommensurate Phases in Dielectrics" ed. R.Blinc and A. P. Levanyuk , vol. **14.1**, chapt. **4** , (North Holland, Amsterdam 1986).
[8] W.Zapart, Ferroelectrics 97, 137 (1989)
[9] A.M. Ziatdinov, V.G. Kuriavyi, R.L. Davidivitch, Solid State Physics, **27**, 2152 (1985)
[10] M.Suhara, T. Bandoh, T.Kitai, Phase Transitions 37, 111 (1992)

Random Orientation ESR Studies of Spin Alignment in High-Spin Carbenes of Heteroatomic π-Conjugation

Jae Young Bae[a], Masafumi Yano[a], Kazunobu Sato[a], Daisuke Shiomi[b], Takeji Takui[a], Takamasa Kinoshita[a], Kyo Abe[a], Koichi Itoh[b], and Daeil Hong[c]

[a]Department of Chemistry and [b]Department of Material Science
Faculty of Science, Graduate School of Science
Osaka City University, Sumiyoshi-ku, Osaka 558-8585, Japan
[c]Department of Chemistry, Collage of Natural Science
Keimyung University, Dalseo-ku, Taegu 704-701, Korea

Contents

I. Abstract

Spin alignment of heteroatomic π-conjugated systems, 2,6-, 2,4-, and 3,5-pyridine-bis (phenylmethylene) (3,5-PY), in which heterocycle plays a ferromagnetic or antiferromagnetic linker between carbenic units, has been studied by random orientation ESR spectroscopy. The electronic structures of the isomers are important for the understanding of spin alignment vs. topology of the heteroatomic π-electron networks. In 2,6-PY and 2,4-PY, the perturbing nitrogen atoms are in active positions, giving rise to a larger influence on their spin structure than in 3,5-PY. A simple application of molecular Hund's rule is invalidated.

II. Introduction

Organic molecule-based magnetics has been the topic of increasing interest in many fields of both the pure and applied sciences for the last three decades. This research field is based on high-spin chemistry which can date back to the first detection of a quintet organic molecule, *m*-phenylenebis(phenylmethylene) (**I**) by K. Itoh (1) and E. Wasserman *et al.* (2) in 1967, demonstrating the importance of the topological nature of homoatomic (carbon) π-electron networks in generating high-spin ground states of organic systems (3-5).

We have studied the topological nature of the heteroatomic (nitrogen) π-electron networks in organic high-spin systems. We focus our attention on isomers in which the heterocycle plays the role of either a ferromagnetic or antiferromagnetic linker between carbenic units (6). The electronic structures of the isomers are of fundamental importance for the understanding of spin alignment vs. topology of the heteroatomic π-electron networks in organic high-spin systems.

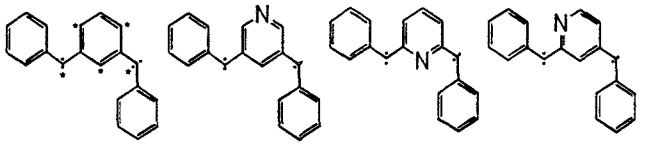

I 3,5-PY 2,6-PY 2,4-PY

In alternant hydrocarbons (AH) the carbon sites can be divided into two sets, * and non-*, such that no two members of the same set are connected. Note that in 3,5-PY the nitrogen atom is at a non-active (non-*) site of the corresponding AH, and in both 2,6-PY and 2,4-PY the nitrogen atom is at an active (*) site. In 2,6-PY and 2,4-PY the perturbing nitrogen atoms in active positions impose a larger influence on their spin structure than in 3,5-PY.

III. Experimental

The diazo precursors of the isomers were fairly soluble in 2-MTHF (2-methyltetrahydrofuran). The solutions of these diazo precursors were degassed by freeze-pump thaw cycles and sealed off on a vacuum line. The sample tubes were set at the sample site of a cryostat at cryogenic temperature. The glassy samples were irradiated for 60 minutes at 10 K with 436 nm light selected by a glass filter (Toshiba KL440) placed in front of a SAN-EI UVF-351S 300W high-pressure mercury lamp. The sample preparation was carried out in the dark.

IV. Results and Discussion

Random Orientation ESR Spectra We detected the quintet ESR signals after photolysis of 3,5-PY below 10K in 2-MTHF. However, both 2,6-PY and 2,4-PY showed only triplet ESR spectra after photolysis below 10K in 2-MTHF. The triplet signals were due to monocarbenes as by-products generated by side reactions. All the observed results suggest that the ground states of both 2,6-PY, and 2,4-PY are singlet while that of 3,5-PY is quintet.

The best fit spin Hamiltonian parameters of the two spectra for 3,5-PY were found to be S = 2, g = 2.003 (isotropic), $|D_1| = 0.0719\ cm^{-1}$, $|E_1| = 0.0198\ cm^{-1}$ (conformer 1) and S = 2, g = 2.003 (isotropic), $|D_2| = 0.1192\ cm^{-1}$, $|E_2| = 0.0063\ cm^{-1}$ (conformer 2). We have detected for the first time the quintet ESR signals from the two conformers which coexist after photolysis of 3,5-PY below 10K in 2-MTHF (Fig. 1). The fine structure parameters and the |E/D| ratio for conformer 1 (*cis-trans* type) and conformer 2 (*trans-trans* type) of 3,5-PY were reproduced by a semiempirical calculation (7) assuming the bond angle (150°) of the divalent carbon atom and molecular conformations.

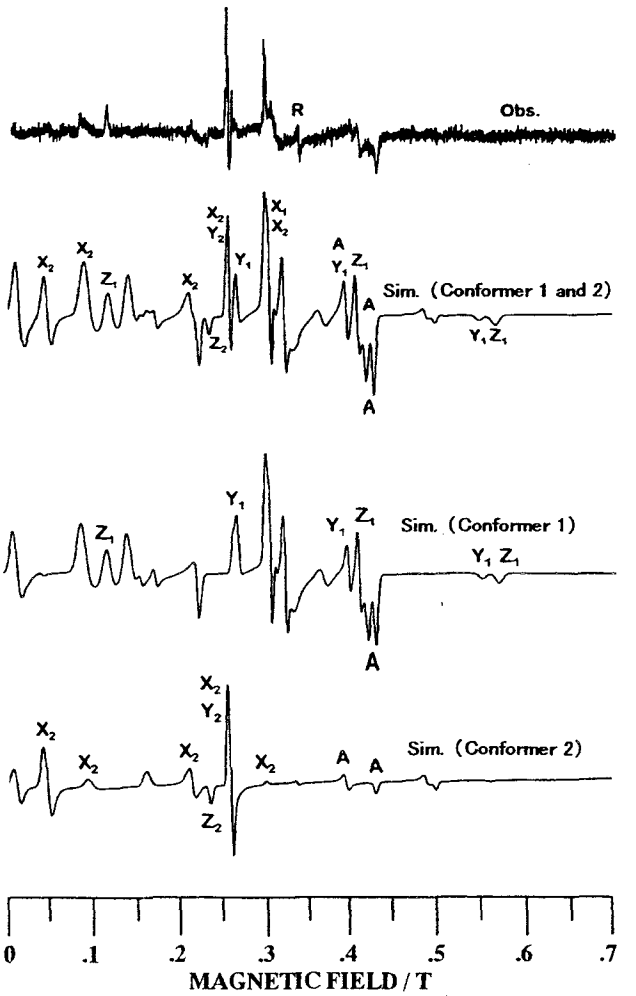

Figure 1. Observed (top) and simulated random orientation ESR spectra for the quintet state of 3,5-PY in 2-MTHF at 10K. The symbol A in the simulated spectrum denotes the off axis extra lines. The symbol R designates doublet species as by-products.

On the other hand, both 2,6-PY and 2,4-PY showed only triplet ESR spectra from monocarbenes after the photolysis (Figs. 2 and 3). The observed fine-structure constants for 2,6-PY and 2,4-PY (two conformers) were $|D| = 0.3341$ cm^{-1}, $|E| = 0.0155$ cm^{-1}, and $|D_1| = 0.3811$ cm^{-1}, $|E_1| = 0.0170$ cm^{-1}, and $|D_2| = 0.3539$ cm^{-1}, $|E_2| = 0.0194$ cm^{-1}, respectively.

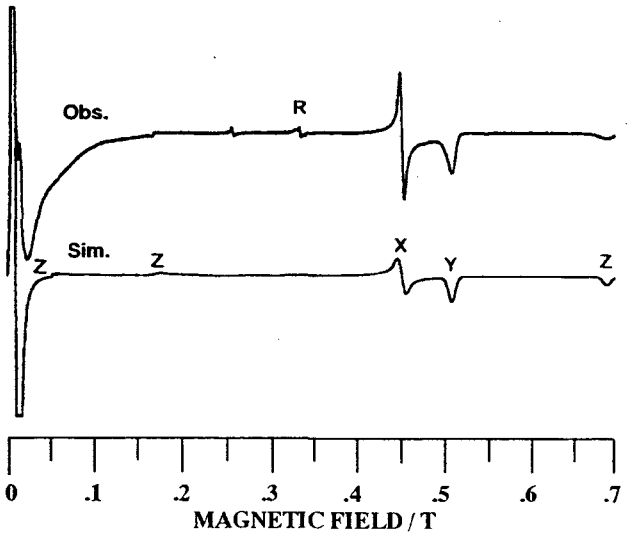

Figure 2. Observed (top) and simulated random orientation ESR spectra for the triplet state of the monocarbene of 2,6-PY in 2-MTHF at 10K.

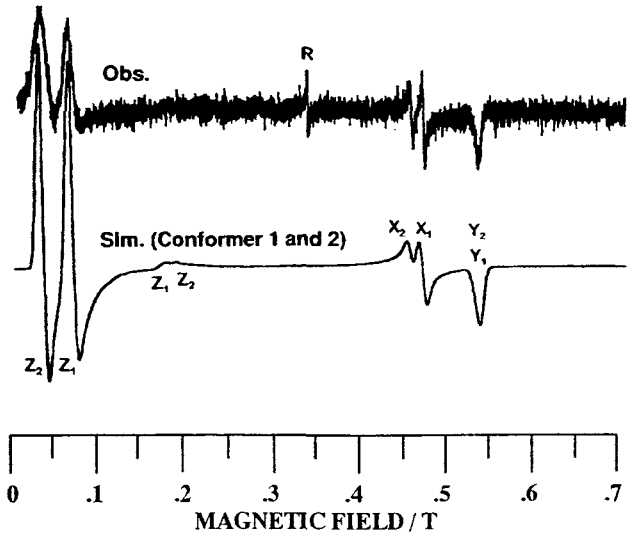

Figure 3. Observed (top) and simulated random orientation ESR spectra for the triplet states of the monocarbene of 2,4-PY in 2-MTHF at 10K.

Molecular Orbital Theory The prominent effect of the heteroatomic replacement appears in the energies of two degenerate π-NBMOs (non-bonding molecular orbital) for 3,5-PY and of two quasi degenerate π-MO's appearing nearby zero energy in units of β for 2,6- and 2,4-PY. In 3,5-PY where the nitrogen atom is at a non-active site, the electronic structure of 3,5-PY is quite similar to **I** and the energy gap between Ψ_{10} and Ψ_{11} is zero. However, in 2,6- and 2,4-PY where the nitrogen atoms are at active sites, the heteroatomic perturbation imposes a larger influence on their spin structures than on that of 3,5-PY; as a result the energy gaps become non-zero. We obtained in terms of a simple molecular orbital calculation that the energy gap of 3,5-PY as well as of **I** is zero whereas those of 2,6- and 2,4-PY are 0.107β

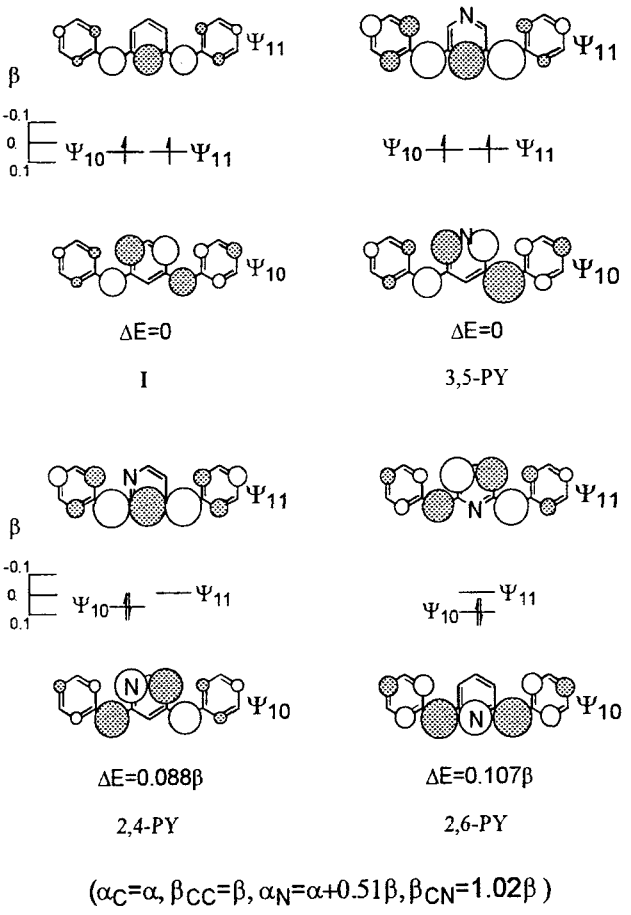

Figure 4. Zero and nearby zero orbital energy diagram for **I**, 3,5-, 2,6- and 2,4-PY calculated by the simple MO theory.

and 0.088β, respectively (Fig. 4). These tendencies favor parallel spins for 3,5-PY and **I** but antiparallel spins for 2,6- and 2,4-PY in the ground state. As mentioned above, all the observed and calculated results show that the ground state of 3,5-PY is quintet whereas those of 2,6- and 2,4-PY are singlet.

Valence Bond Approach in Terms of the MO Calculation We illustrate the valence bond (VB) approach (8-10) for the interpretation of the open-shell electronic structure and spin alignment of organic high-spin systems. It should be noted that the numerical results obtained here depend on the level of MO calculations. An advantage of this methodology is that the spin structure associated with spin alignment can be described in a systematic and quantitative manner and that a translation from the MO to the VB is free from the method picture in the MO calculation. The relative contributions of dominant spin structures (S=1) of wavefunctions obtained by the simple MO calculations for **I**, 3,5-PY, 2,6-PY and 2,4-PY are 1.95, 1.92, 1.88, and 1.89, respectively (See the top line of Fig. 5). The results clearly demonstrate that the progression **I** → 3,5-PY → 2,4-PY → 2,6-PY represents a preferential stabilization of the triplet relative to the singlet (Fig. 5).

As is generally the case with biradical systems, both VB and MO arguments can be developed. Arguments based on MO theory emphasize the role of the NBMOs. In 3,5-PY, nitrogen atom is introduced at a position where there are negligible coefficients of atomic orbitals in both NBMOs. Hence, very little perturbation occurs, and 3,5-PY behaves like **I**. In both 2,6-PY and 2,4-PY, however, nitrogen atom is at a site that has a large coefficient in one NBMO, and a negligible coefficient in the other.

Gaussian 94 (DFT calculations) We calculated the singlet (excited state)-quintet (ground state) [abbreviated to S-Q] gaps of the three isomers as well as **I** using geometry optimizations. The calculations were performed with the Gaussian 94 package of *ab initio* programs. The S-Q gap of 3,5-PY (*trans-trans*; 3.08×10^{-2}, *cis-trans*; 3.03×10^{-2} Hartree) showed very little heteroatomic perturbation which resembles the S-Q gap of **I** (3.08×10^{-2} for *trans-trans*, 2.97×10^{-2} Hartree for *cis-trans*) (1 Hartree = 627.51 kcal/mol). However, the S-Q gaps of 2,6-PY and 2,4-PY exhibited larger heteroatomic perturbation than that of **I**. The S-Q gaps of 2,6-PY and 2,4-PY are 3.49×10^{-2} for *trans-trans*, 3.64×10^{-2} for *cis-trans*, and 3.62×10^{-2} for *trans-trans*, 3.61×10^{-2} for *cis-trans*, 3.37×10^{-2} Hartree for *trans-cis*. These molecular structures of 3,5-PY and 2,4-PY obtained by the geometry optimization were depicted in Fig. 6. The results assist the MO and VB approaches mentioned above.

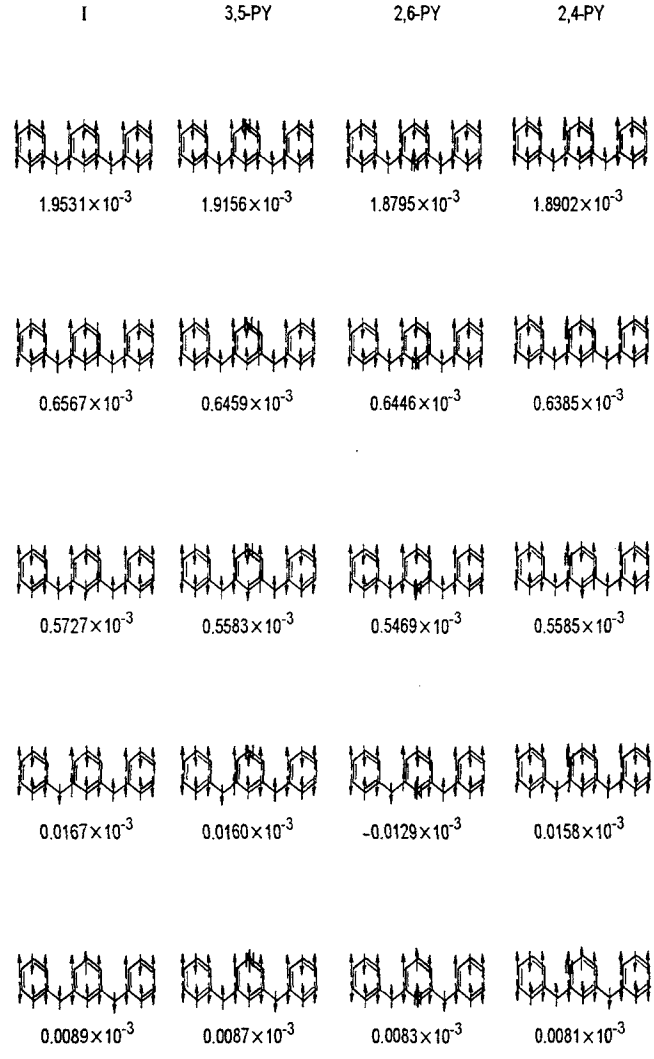

Figure 5. Relative contribution of dominant spin structures calculated by a VB approach in terms of the simple MO calculation.

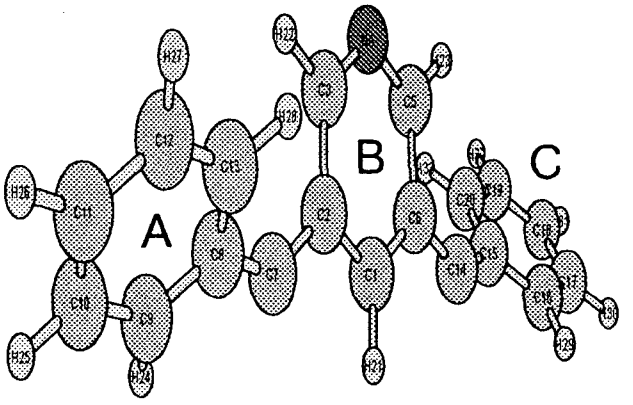

Dihedral angle between A and B: **-50.50°**
Dihedral angle between B and C: **-50.58°**

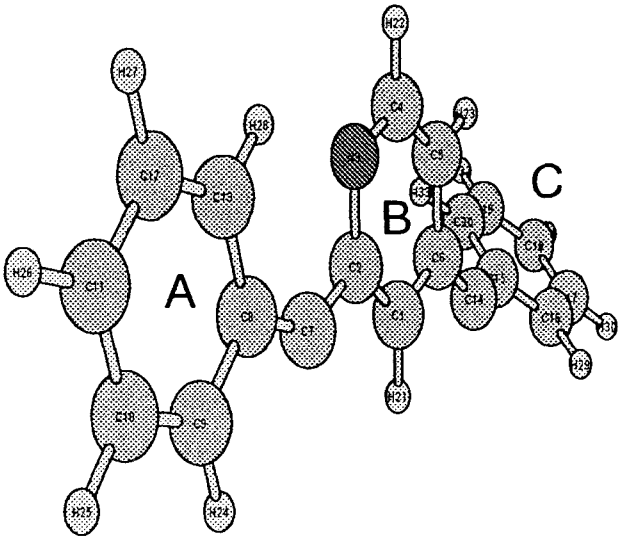

Dihedral angle between A and B: **-0.33°**
Dihedral angle between B and C: **-49.99°**

Figure 6. Molecular Structures of 3,5- and 2,4-PY Calculated by *Gaussian 94* (DFT calculations)

V. Conclusion

We concluded that 3,5-PY is in the quintet ground state. The two conformers of 3,5-PY were identified. However, both 2,6-PY and 2,4-PY showed only triplet ESR spectra after the photolysis. The triplet signals are attributed to the ground-state triplets of monocarbenes as by-products generated by side reactions. In 2,6-PY and 2,4-PY the perturbing nitrogen atoms are in active (*) positions, imposing a larger influence on their spin structures than in 3,5-PY where the nitrogen atom is in non-active position. These findings suggest that 2,6-PY and 2,4-PY are spin-singlet in the ground state in agreement with the MO and VB approaches, and with interpretation in terms of *Gaussian 94* (DFT calculations). The simple extension of "π-topology rule for spin alignment in homoatomic π-systems" is invalidated for that in heteroatomic π-systems.

VI. Acknowledgments

This work was supported by Grants-in-Aid for Scientific Research on Priority Area "Molecular Magnetism" (Area No. 228/04 242 103 and 04 242 105) from the Ministry of Education, Science and Culture, Japan and also by NEDO Project "Organic Magnets" from the Ministry of International Trade and Industries, Japan.

VII. References

[1] K. Itoh, *Chem. Phys. Lett.*, **1**, 235 (1967).

[2] E. Wasserman, R. W. Murray, W. A. Yager, A. M. Trozzolo, and G. Smolinsky, *J. Am. Chem. Soc.*, **89**, 5076 (1967).

[3] T. Takui and K. Itoh, *Chem. Phys. Lett.*, **19**, 120 (1973).

[4] K. Itoh, *Pure Appl. Chem.*, **50**, 1251 (1978).

[5] *Molecular Magnetism ed.* by K. Itoh, Gakkai Publishing Center (1996).

[6] A. P. West, Jr., S. K. Silverman, and D. A. Dougherty, *J. Am. Chem. Soc.*, **118**, 1452 (1996).

[7] J. Y. Bae, *Ph. D. Thesis*, Osaka City University (1998).

[8] W. Moffitt, *Proc. Roy. Soc.*, **Ser. A 218**, 486 (1953).

[9] K. Sato, *Ph. D. Thesis*, Osaka City University (1994).

[10] T. Takui and P. Kalafiloglou, unpublished.

Solution and Solid-state Vanadium-51 NMR Studies of Dioxovanadate(V) Complexes

Man-Ho Lee and Shigenobu Hayashi[1]
Department of Industrial Chemistry, Kyungpook National University, Taegu 702-701, Korea
[1]National Institute of Materials and Chemical Research, Tsukuba, Ibaraki 305, Japan

INTRODUCTION

In recent years ^{51}V NMR has emerged as a powerful tool for studying the local environment of ^{51}V nuclei in solution[1] and solid-state.[2] The ^{51}V nucleus (spin I = 7/2, natural abundance 99.76%) has an electric quadrupole moment which interacts with the gradient of the intramolecular electric field. This interaction produces the so called quadrupolar effects of the first and second order in ^{51}V NMR spectra.[3] The analysis of these effects allows one to measure the quadrupolar coupling constant e^2qQ/h and asymmetry parameter η_Q These parameters directly characterize the gradient of the electric field which is created at the V nucleus by the surrounding atoms and thus can be related to distortions of the symmetry of the local environment of the V atom. As found recently, the principal components of the chemical shift tensor are also very sensitive to the type of local environment of ^{51}V nuclei.[4]

In general, three different types of interaction influence the ^{51}V NMR spectra of solid diamagnetic samples: (1) the dipole interaction of the magnetic moment of the ^{51}V nucleus with magnetic moment of other nuclei, leading to broad lines; (2) the quadrupolar interaction of the ^{51}V nuclei with the electric field gradient, which splits the lines and contributes to the shift of the central (m_I=1/2 $\leftrightarrow$ -1/2) lines; (3) the chemical shift interaction, which changes the position of the lines and makes them asymmetric. The line shape can be rather complicated due to simultaneous action of all three types of interaction. The dipolar interaction and the first order quadrupolar interaction do not depend on the spectrometer frequency ν_0, while the second order quadrupolar effects are inversely proportional to ν_0 The effects of the anisotropy of the chemical shift are directly proportion to ν_0 Thus, at high enough ν_0 the second order quadrupolar effects are suppressed and can be neglected, while the effects of the chemical shift anisotropy become more pronounced and can be measured more precisely.

In this paper, we measure the chemical shift anisotropies and the quadrupolar coupling interactions of ^{51}V nuclei in several dioxovanadate(V) complexes from magic-angle-spinning (MAS) spectra of the powder samples. In our knowledge this is the first report to measure the chemical shift anisotropy and the quadrupolar coupling constant of ^{51}V in vanadium(V) complex.

EXPERIMENTAL

Materials

All reagent grade chemicals were used as received without further purification. Ammonium metavanadate, oxalic acid (H_2Ox), ethylenediaminetetraacetic acid (H_4EDTA), nitrilotriacetic acid (H_3NTA), and propylenediaminetetraacetic acid (H_4PDTA) were obtained from Aldrich Chemical Co. Dioxovanadate (V) complexes were prepared from the reaction of ammonium metavanadate and ligand in aqueous solution with the similar method reported elsewhere.[5]

NMR measurements

Solution ^{51}V spectra of samples in H_2O-D_2O (90:10 v/v) were recorded on a JEOL GSX-400 spectrometer (105 MHz) at room temperature. Spinning (MAS and off-MAS) ^{51}V spectra of powder samples were recorded on a Bruker MSL-400 spectrometer (105.25 MHz) at room temperature. Bruker high-speed probehead was used with rotors of 4 mm o.d. The angle in the off-MAS measurements was chosen so that the intensities of the spinning sidebands caused by the satellite transitions were negligible. The spinning axis used was inclined at 53.7 ° to the magnetic field. The spinning rate for MAS spectra was 10 kHz. The ordinary single pulse sequence with phase alternation was used with and without ^1H high-power decoupling during signal acquisition. ^1H high-power decoupling had negligible effect on the line shape. The $\pi/2$ pulse width for solution was set at 6.0 μs The pulse length

was 1.0 μ s and the repetition time was 1.0 s. Recovery time after the pulse transmission was 5 μs The chemical shifts were referenced to external $VOCl_3$. Details of the measurements were described in the previous paper.[6]

Analysis of the Solid-state ^{51}V Spectra

The line shape of the spectra and the intensity of the spinning side bands (SSBs) were analyzed using our own softwares written in Fortran. The powder averaging procedure incorporates the two-dimensional interpolation and partitioning all directions presented by Alderman *et al.*[7] The intensity of SSBs in MAS spectra produced by chemical shift anisotropy was calculated using the formula derived by Herzfeld and Berger.[8] Chemical shift anisotropy was estimated from the SSB intensity using a least squares fitting,[9] in which the procedure was based on Fenzke *et al.*[10] The detailed procedure is described elsewhere.[11]

RESULTS AND DISCUSSION

Solution ^{51}V NMR spectroscopy

The complexes show ^{51}V peaks whose chemical shifts fall in the range of -503.5 and -534.4 ppm relative to $VOCl_3$ as shown in Table 1, indicating octahdral geometry.[1] The half-widths of oxalate complexes are smaller than other complexes, due to the increase of symmetry in the structure of oxalate complexes. PDTA complex show two ^{51}V peaks at -503.5 and -515.5 ppm, indicating isomerization of the complex in aqueous solution.

Table 1. ^{51}V chemical shifts of dioxovanadate(V) complexes in solution

Complex	δ (ppm)[a]	Half-width (Hz)
$(NH_4)_2[VO_2NTA]$	-504.3	480
$(NH_4)_3[VO_2PDTA]\ H_2O$		
(I)	-503.5	1290
(II)	-515.5	1050
$(NH_4)_3[VO_2EDTA]$	-517.7	910
$Na_3[VO_2EDTA]\ 4H_2O$	-518.0	960
$(NH_4)[VO_2H_2EDTA]\ 3H_2O$	-524.3	1150
$(NH_4)_3[VO_2Ox_2]$	-534.4	290
$K_3[VO_2Ox_2]\ 3H_2O$	-534.1	320

[a]Relative to external $VOCl_3$.

Solid-state ^{51}V NMR spectroscopy

Magic angle spinning (MAS) can average the broadening effect of the first-order quadrupole interaction, giving rise a large number of SSBs. Chemical shift anisotropy is also averaged by MAS, which also results in SSBs. Therefore, one can estimate the quadrupole coupling and the chemical shift anisotropy from analysis of the SSB intensity.[12]

MAS and off-MAS ^{51}V spectra of the powder $(NH_4)_2[VO_2NTA]$ are shown in Fig. 1 (a). A large number of spinning sidebands are observed over a range wider than 1.0 MHz, which originate mainly from the satellite transitions broadened by the first-order quadrupole interaction. Several stronger signals in the central position might be originated from the central transition. The large shielding anisotropy at high magnetic field (9.4 T) causes the MAS spectra to be broken up into centerbands and an extensive set of spinning side bands, which are spaced by integer multiples of the spinning

Table 2. Parameters of chemical shift anisotropy and quadrupole coupling of ^{51}V

Complex[a]	δ_{iso} (ppm)	$\Delta\delta_a$ (ppm)	η_c	e^2qQ/h (MHz)	η_Q	α (deg.)	β (deg.)	γ (deg.)	δ_{sol} (ppm)
1	-507.0	-800	0.04	8.80	0.75	0	3	0	-504.3
2	-502.0	-760	0.06	7.50	0.33	0	0	0	-503.5 -515.5
3	-518.4	-720	0.06	7.50	0.50	0	2	0	-517.7
4	-513.0	-800	0.06	8.75	0.49	0	3	0	-518.0
5	-480.8	-870	0.06	9.16	0.48	0	0	0	-524.3
6	-534.0	-730	0.28	7.84	0.50	0	5	0	-534.4
7	-547.4	-740	0.28	8.15	0.70	0	10	0	-534.5
Error	0.5	10	0.02	0.05	0.02	30	2	30	0.5

[a]1; $(NH_4)_2[VO_2NTA]$, 2; $(NH_4)_3[VO_2PDTA] \cdot H_2O$, 3; $(NH_4)_3[VO_2EDTA]$, 4; $Na_3[VO_2EDTA] \cdot 4H_2O$, 5; $NH_4[VO_2H_2EDTA] \cdot 3H_2O$, 6; $(NH_4)_3[VO_2\ Ox_2] \cdot 4H_2O$, 7; $K_3[VO_2Ox_2] \cdot 3H_2O$.

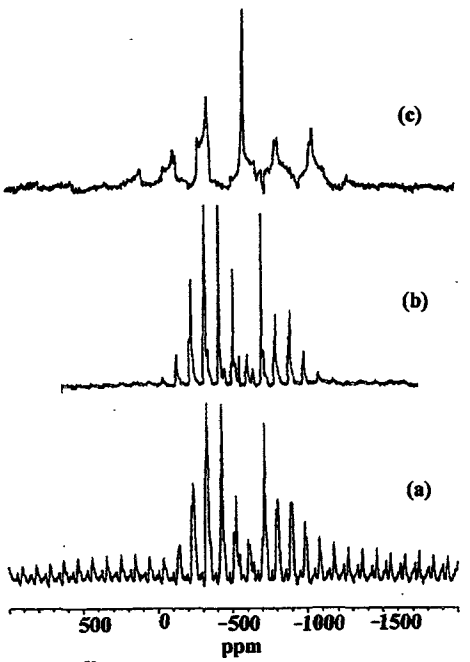

Fig. 1. ^{51}V NMR spectra of the powder $(NH_4)_2[VO_2NTA]$. (a)MAS and (b) off-MAS spectra measured at 105.25 MHz and (c)off-MAS spectra at 52.64 MHz. The spinning rates were (a, b) 10.00 kHz (c)12.00 kHz.

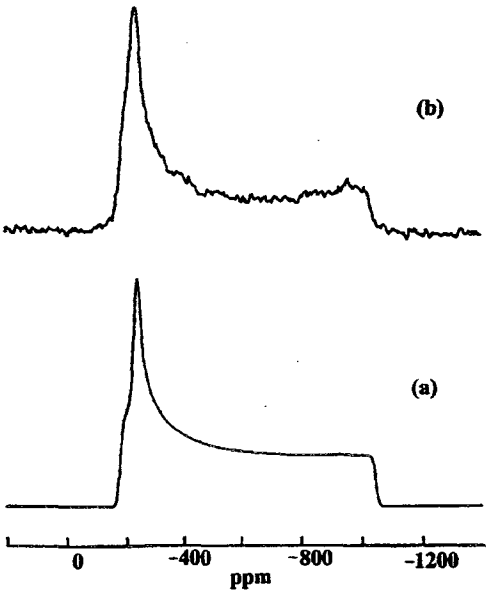

Fig. 2.(a)Calculated and (b)observed static 51V NMR spectra of the powder $(NH_4)_2[VO_2NTA]$ at 105.25 MHz.

frequency. We cannot separate the central transition from the atellite transitions due to the severe overlapping. Thus, we measured off-MAS ^{51}V spectra, as shown in Fig. 1(b, c) to obtain only the signals from the central transitions.[13] These signals are ascribed to the central transition. The first-order quadrupole interaction does not work on the central transition (+1/2 ↔ -1/2), and therefore the chemical shift anisotropy and the second-order quadrupole interaction influence the line shape and the chemical shift of ^{51}V signal. We analyzed the SSB intensities and line shapes of the off-MAS spectra to obtain chemical shift anisotropy and the quadrupole coupling data, summarized in Table 2.

We have also measured the ^{51}V spectra for static samples as shown in Fig. 3. Static signals from the satellite transitions are not clearly observed and the line shape of the central transition is governed dominantly by chemical shift anisotropy. We have simulated the static spectra to check and confirm validity of the parameters obtained from analyses of the off-MAS spectra.

Dioxovanadate (V) complexes show the large chemical shift anisotropy ($\Delta\delta_a$ = -800 ~ -720 ppm) for ^{51}V atom. The components of the ^{51}V chemical shift tensor are very sensitive to the type of atoms in the first coordination sphere of the V atom. The isotropic chemical shifts (δ_{iso}) of the solid samples are very close to the values (δ_{sol}) obtained from solution. ^{51}V resonance peak in solid-state is essentially not shifted in frequency from the solution value except by outer-sphere interaction. It is interesting to note the nearly axial symmetry of chemical shift tensors, which reflect similar deshielding environments for both nitrogen and oxygen donor atoms. The stronger the distortion from a regular octahedron, the larger the value of $\Delta\delta_a$ The values of eulerian angles (α, β, γ) indicate that the principal axes of chemical shift tensor and quadrupole interaction tensor are almost the same. Distortion of octahedron results in an increase of the electric field gradient at V nucleus, giving large quadruploe coupling constant (e^2qQ/h = 7.50 ~ 9.16 MHz) in the complexes. It seems to expect a correlation between $\Delta\delta_a$ and quadrupole coupling for the complexes. The static ^{51}V spectrum of a single crystal is shown in Fig. 3, indicating two distinquishable signals which means two magnetically inequivalent but chemically identical vanadium sites. These sites are generated by the 2_1 symmetry operator within the unit cell.[6]

Acknowledgment - This work was partially supported by the Korea Science and Engineering Foundation (grant number 971-0304-025-2).

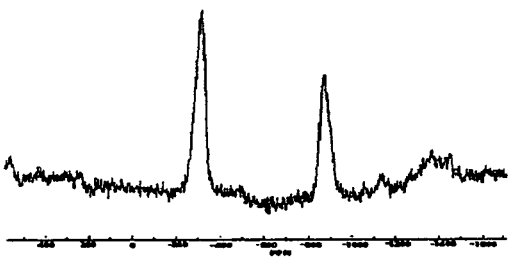

Fig. 3. Static ^{51}V NMR spectra of the single crystal $(NH_4)_2[VO_2NTA]$ at 105.25 MHz.

REFERENCES

1. O. W. Howarth, *Prog. NMR Spectrosc.* **22**, 43 (1990) and references are therein.
2. O. B. Lapina, V. M. Mastikhin, A. A. Shubin, V. N. Krasilnikov, and K. I. Zamaraev, *Prog. NMR Spectrosc.* **24**, 457 (1992) and references are therein.
3. D. Rehder, *Bull. Magn. Reson.* **4**, 33 (1982).
4. H. Eckert and I. E. Wachs, *J. Phys. Chem.* **93**, 6796 (1989).
5. L. Przyborowski, G. Schwarzenbach, and Th. Zimmermann, *Helv. Chim. Acta*, **48**, 1556 (1965).
6. M. -H. Lee, N. H. Heo and S. Hayashi, *Polyhedron*, **17**, 55 (1998).
7. D. W. Alderman, M. S. Solum, and D. M. Grant, *J. Chem. Phys.*, **84**, 3717 (1986).
8. J. Herzfeld and A. E. Berger, *J. Chem. Phys.*, **73**, 6021 (1980).
9. S. Hayashi and K. Hayamizu, *Chem. Phys.*, **157**, 381 (1991).
10. D. Fenzke, B. Maess, and H. Pfeifer, *J. Mag. Reson.*, **88**, 172 (1990).
11. S. Hayashi, *Magn. Reson. Chem.*, **34**, 791 (1996).
12. M. Mehring, "Principles of High Resolution NMR in Solids" Springer-Verlag, Berlin, 1983.
13. E. Oldfield, R. A. Kinsey, B. Montez, T. Ray and K. A. Smith, *J. Chem. Soc. Chem. Commun.*, 254 (1982).

Weak Exchange Effect in EPR Spectrum of $[N(CH_3)_4]_2MnBr_4$

J.Solecki, W.Zapart, M.B.Zapart, K.Tanaka[1] and A.Sawada[2]
Institute of Physics, Technical University, 42-200 Czestochowa, Poland
[1] Electr. Res. Lab., Matsushita Electronic Corporation, Osaka 569-11, Japan
[2]Dept. of Physics, Faculty of Science , Okayama University, Okayama 700, Japan

1.Introduction

Structural and magnetic properties in a group of crystals belonging to the family A_2BX_4 have gained much interest in the last few years. These crystals show the presence of numerous phase transitions related to the structural reorganisation of BX_4 tethraedra [1]. Different approaches have been used to characterise these complexes. Among them, Electron Paramagnetic Resonance (EPR) studies allow to get important information related to the nature of magnetic as well as structural properties of these species [2].

Our interest concentrates on two species of A_2BX_4 family, $[P(CH_3)_4]_2MnBr_4$ and $[N(CH_3)_4]_2MnBr_4$. These two crystals are isomorphous with an analogous phase transition scheme leading from a normal phase of orthorhombic symmetry (Pmcn, Z=4) to a ferroelastic phase of monoclinic symmetry (P121/c1)[3,4]. Our earlier investigations of $[N(CH_3)_4]_2MnBr_4$ and $[P(CH_3)_4]_2MnBr_4$ revealed that the EPR spectra of Mn^{2+} were sensitive to the structural phase transition in these compounds [6,7]

It is well known that positions, line shapes and line widths of EPR lines in magnetically concentrated systems to which these crystals belong are influenced by development of the short range interactions in the spin system. The observed EPR spectra of $[P(CH_3)_4]_2MnBr_4$ and $[N(CH_3)_4]_2MnBr_4$ exhibit poorly resolved line or only a single EPR line, depending on the orientation of the external magnetic field. In this paper the results of measurement of the linewidth and lineshape on single crystal $[N(CH_3)_4]_2MnBr_4$ are presented.

Single crystals of pure $[N(CH_3)_4]_2MnBr_4$ of bright green colour are obtained by slow evaporation at 30°C from HBr acidic aqueous solutions

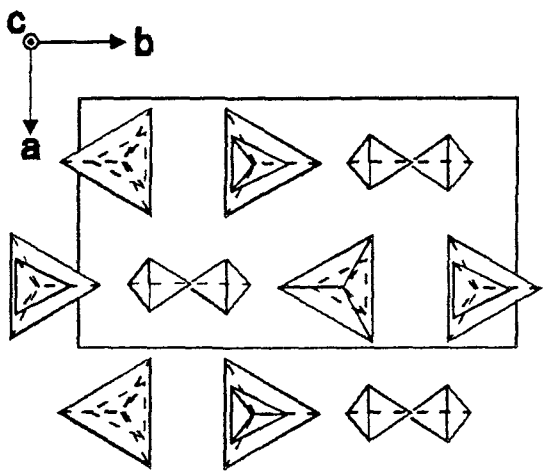

Fig.1. Projection of the structure of $[N(CH_3)_4]_2MnBr_4$ along the [001] direction. The pseudohexagonal arrangement of $MnBr_4$ and $N(1)(CH_3)_4$ is indicated by bold large and small tetrahedra, while the light small tetrahedra represent $N(2)(CH_3)_4$; the apices represent positions of Br or C atoms.

containing stoichiometric amounts of $N(CH_3)_4Br$ and $MnBr_2 \cdot H_2O$.

The crystal structure projected along the [001] axis shows a pseudohexagonal arrangement of tetrahedral ions [Fig. 1]. The distortion of $MnBr_4$ is relatively small. In its low-temperature phase the structure of crystal is characterised by two kinds of chains composed of $MnBr_4$ and $N(1)(CH_3)_4$; one is along the [001] axis and the other is along the [100] axis [9].

2. Experimental

The EPR spectra are obtained with a conventional spectrometer at the X-band (9.3 GHz). Single crystal of $[N(CH_3)_4]_2MnBr_4$ are selected for their high crystalline quality and orientated according to the given morphology [Fig. 2]. The

crystal was rotated around the c axis as well as around non–crystallographic directions.

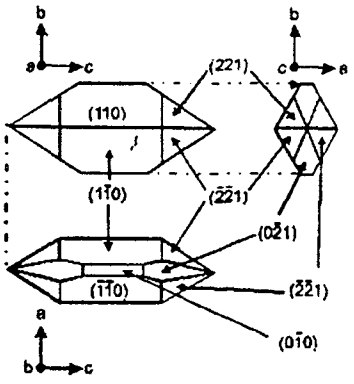

Fig. 2. The morphology and crystallographic axes of [N(CH)] MnBr

3. Results

Observed spectra exhibit partially resolved EPR line or only a single EPR line, depending on the orientation of the crystal in the external magnetic field.

Fig. 3 presents an example of EPR spectrum of Mn^{2+} in $[N(CH_3)_4]_2MnBr_4$ when partially resolved EPR lines could be observed. In this case a good agreement between observed and simulated spectra has been obtained, when one assumes that EPR spectrum consists of at least four lines of gaussian shape what is shown at the bottom of this figure.

Usually EPR spectra of Mn^{2+} consist of five lines of fine structure and each of this lines splits into six lines of hyperfine structure. It gives thirty lines which comes from allowed transitions. There is further multiplication of the number of the lines when there are some manganese ions in magnetically or structurally unequivalent sites.

The EPR lines in $[N(CH_3)_4]_2MnBr_4$ are considerably broadened what leads to vanishing of the hyperfine structure and overlapping of the fine structure lines. Because $[N(CH_3)_4]_2MnBr_4$ is a dense paramagnet a broadening can be involved

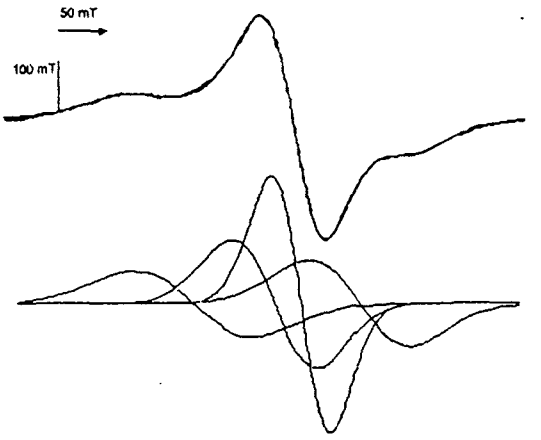

Fig. 3. EPR spectrum of Mn^{2+} in $[N(CH_3)_4]_2MnBr_4$ and its decomposition into four components

by dipole-dipole and exchange interactions. As the dipole-dipole interaction broadenes the resonance lines the strong enough exchange interaction can narrow them. Observed width of the

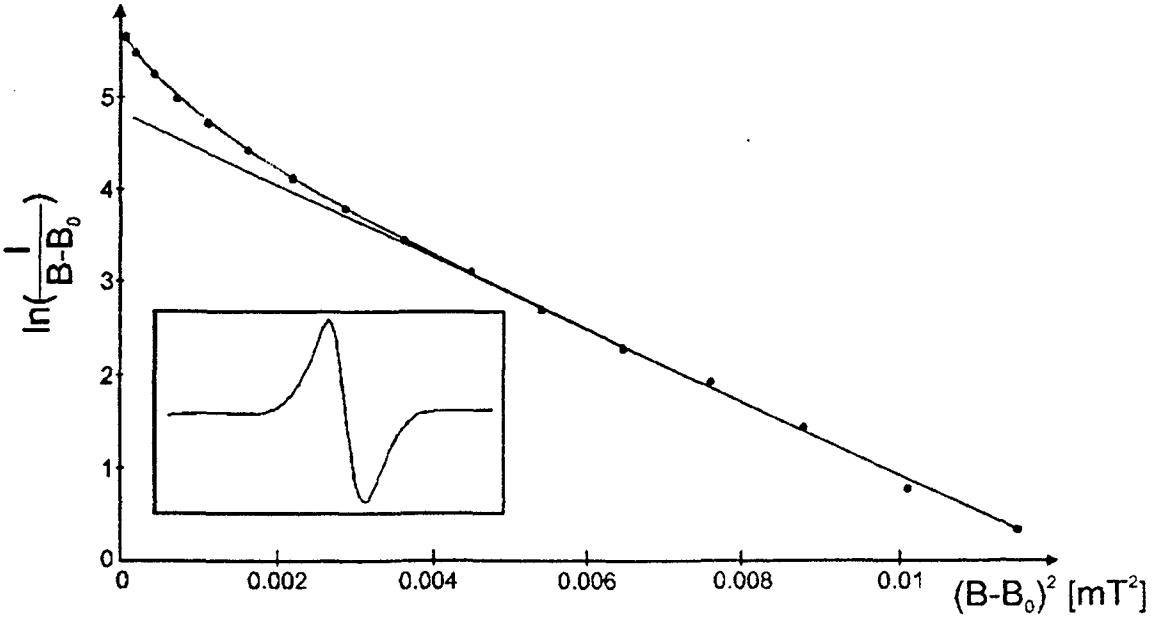

Fig. 4. Linearization of the experimental data using gaussian formula. In the inset the analysed EPR line is shown

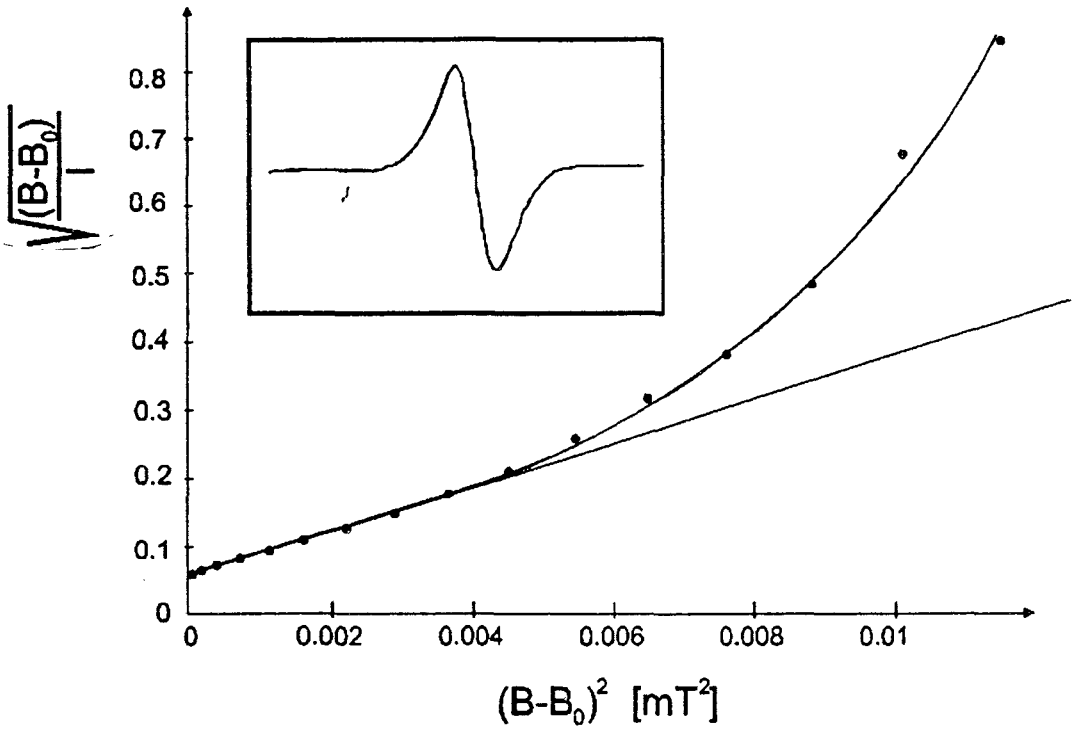

Fig. 5. Linearization of the experimental data using lorenzian formula. In the inset the analysed EPR line is shown

resonance lines is about of 50 mT what can be

Tab. 1. Parameters characterising the EPR spectrum of Mn^{2+} in $[N(CH_3)_4]_2MnBr_4$ crystal

	Parameters obtained from the left side of the line	Parameters obtained from the right side of the line
B_e [T]	0.0669	0.0670
ν_e [GHz]	1.87	1.87
ΔB^G [T]	0.0521	0.0526
ΔB^L [T]	0.0385	0.0457
$\frac{(\Delta B^G)^2}{\Delta B^L \cdot B_e}$	1.053	0.903
g	2.00	
D	0.04	

the evidence of lack of the strong exchange interaction.

Therefore we could assume that the exchange interaction is weak enough to make possible the observations of the non-equivalent manganese centres (four $MnBr_4$ thetraedras in each cell). In order to study exchange effects on EPR line shape a spectrum in a form of one resonance line has been chosen for the analysis.

The lineshapes have been analysed as usually by plotting the quantity $[(B-B_0)/I]^{1/2}$ versus $(B-B_0)^2$ for the Lorentzian line and $\ln[I/(B-B_0)]$ versus $(B-B_0)^2$ for the Gaussian one, where I is the amplitude of the first derivative of the EPR line for the applied static magnetic field B, B_0 is the resonance field. We have made our analyse for left and right side of the experimental line, the results differ slightly but not significantly.

From the plots 4 and 5 we obtain the points of „transition" between lorentzian and gaussian line shape B_e. Thus we can estimate the exchange frequency using relation

$$\nu_e = B_e \cdot g \cdot \beta / h \qquad (1)$$

The estimated exchange frequency as well as „true" line widths of the component lines i.e.

gaussian and lorentzian ones are presented in Tab. 1. To confirm results of the above method one should check if they obey the relation:

$$\frac{\Delta B_G^2}{\Delta B_L \cdot B_e} \approx 1 \qquad (2)$$

The fulfilment of this relation in our case is also shown in this table.

Assuming that the anisotropy of the line positions is due to the fine structure we have tried to estimate the D parameter of the crystal field. Using the spin Hamiltonian of the form [10]

$$H = g\beta H \cdot S + D\left\{S_z^2 - \frac{1}{3}S(S+1)\right\}\left(3\cos^2\theta - 1\right) + \qquad (3)$$

$$D(S_z S_x + S_x S_z)\cos\theta\sin\theta + \frac{1}{4}D(S_+^2 + S_-^2)\sin^2\theta$$

we neglected the terms with hyperfine interaction and nuclear Zeeman energy. Also the non-axial terms in the spin Hamiltonian were not taken into consideration. The highest value of the resonance field obtained from the anisotropy pattern has been assumed as corresponding to the transition between the energy levels |5/2> - |3/2>. This resonance field is equal to about 500 mT. From the energy levels obtained from the first order perturbation theory taking g=2.00 it was possible to estimate value of the D parameter (see Tab.1)

4. Concluding remarks

$[N(CH_3)_4]_2MnBr_4$ is an example of dense paramagnetic in which exchange interaction affect the EPR lineshape. In case of fast exchange, when the exchange frequency is much greater then the separation $\Delta\omega$ between the spectral lines the result is a single line at the average frequency with a width $\delta\omega$ [11]:

$$\delta\omega \approx \frac{(\Delta\omega)^2}{\omega_e} \qquad (4)$$

If the exchange is very slow with $\omega_e << \Delta\omega$ the EPR lines are resolved but broadened with a width

$$\delta\omega \approx \omega_e \qquad (5)$$

The EPR Spectrum extension in the case of resolved line in $[N(CH_3)_4]_2MnBr_4$ is about 0.4 T and the estimated exchange field (Table 1) is 0.067 T. On rotating the crystal in the magnetic field the spectrum changes its extension (even narrowing to a single line) what is the reason that our case cannot be treated as example of very weak exchange. It is also the reason of further complications in EPR spectra analysis.

Acknowledgements

This paper was supported through KBN project 2 PO3B 082 13.

References

[1]. I.D. Axe, M. Izumi, G. Shirane in „Incommensurate Phases in Dielectrics" ed. R.Blinc and A. P. Levanyuk , North Holland, Amsterdam 1986.
[2]. J.J.L. Horikx, A.F.M. Arts, H.W. De Wijn, Physical Review B **37**, 13, (1988).
[3]. A. Sawada and K. Tanaka, J. Phys. Soc. Japan **60**, 3593, (1991).
[4]. A. Sawada and K. Tanaka, Ferroelectrics **172**, 45, (1995).
[5]. J. -Cl. Bissey, N. Filloleau, P. Beziade, Nguyen-Ba Chanh, R. Zouari, A. Daoud **201**, 505, (1997).
[6]. M.B. Zapart, W. Zapart, J. Solecki, K. Tanaka, A. Sawada, Ferroelectrics **101**, 199, (1997).
[7]. W. Zapart, J. Solecki, M.B. Zapart, A. Sawada, K. Tanaka J. Korean Phys. Soc. **32**, S697,(1998).
[8]. K. Hasebe, T. Asahi, Acta Cryst. C**45**, 841, (1989).
[9]. K. Hasebe, T. Asahi, Acta Cryst. C**46**, 759, (1990).
[10]. A. Abragam, B. Bliney, „Electron Paramagnetic Resonance of Transition Ions", Clarendon Press, Oxford 1970.
[11]. P. W. Anderson, P. R. Weiss, Rev. mod. Phys. **25**, 269, (1953).

Fluorine-19 High-Speed MAS and Spin Exchange NMR of Fluoropolymers

Ulrich Scheler

Institut für Polymerforschung Dresden e.V. Hohe Straße 6, D-01069 Dresden, Germany

Abstract

High-speed magic angle sample spinning (MAS) has been used to acquire high-resolution solid-state fluorine-19 NMR spectra of fluoropolymers. Additional information is obtained from two-dimensional spin exchange spectra using radio frequency driven recoupling (RFDR). The information about spatial proximity from these spectra is utilized for the signal assignment and for the study of phase separation in semicrystalline PVDF.

Introduction

Fluorine-19 in some respects is the ideal probe nucleus for NMR. This is due to high receptivity, second only to that of the proton, resulting from the large magnetogyric ratio and a natural abundance of 100%, and the large chemical shift range of about 400 ppm for organic materials. The latter means that the resonance frequency strongly depends on the chemical environment of the nucleus under study. The large magnetogyric ratio and the natural abundance, on the other hand, are the source of very strong dipolar couplings (both homonuclear and heteronuclear), which result in experimental difficulties. These difficulties for a long time prevented the acquisition of high-resolution solid-state NMR of fluorine-19. The fact that the Larmor frequencies of protons and fluorine differ by only 6%, does not allow the application of standard double resonance probes. Hardware developments in recent years, like high-speed MAS and dedicated probes for proton-fluorine double resonance, allowed to overcome these difficulties.

High-speed MAS is used to acquire high resolution solid-state NMR spectra. Under MAS orientation dependent interactions are averaged when the spinning frequency exceeds the strength of the interaction, measured in frequency units. For inhomogeneous interactions, like the chemical shift anisotropy, the spectrum is separated into a narrow isotropic line and a set of narrow spinning sidebands separated by the sample rotation frequency, if the rotation frequency does not exceed the strength of the interaction. For homogeneous interactions like the dipolar coupling the separation into spinning sidebands only occurs at higher sample rotation frequencies. The linewidth decreases with the spinning frequency. The alternative for averaging the dipolar coupling would be multipulse [1, 2], but the large spread of Larmor frequencies, in the present case about 100 ppm, constitutes a severe restriction for the cycle time. High-speed MAS, once available, requires less effort for spectrometer setup.

Experimental

The experiments have been performed on a modified Bruker AMX-300 spectrometer operating at a Larmor frequency of 282 MHz for fluorine. A Bruker CRAMPS probe accepting 2.5 mm rotors allowing for spinning speeds of up to 35 kHz with a power combiner to allow proton-fluorine double resonance experiments has been used. The $\pi/2$ pulse duration was 3 μs with a recycle delay of 2 s.

Results

In Fig. 1 fluorine-19 MAS spectra of FEP, a copolymer of tetrafluoroethylene and

hexafluoropropylene with a content of hexafluoropropylene of about 5% [3] are shown for different spinning speeds. The assignment of the peaks is shown above the frequency axis. As indicated by the dashed lines, the spinning sidebands, separated by the spinning speed, are shifted out as the spinning speed increases.

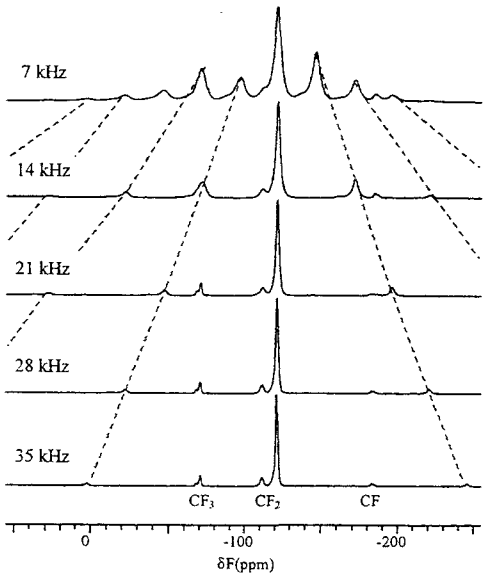

Fig. 1: Fluorine-19 MAS spectra of FEP, sample rotation frequencies as indicated at the slices.

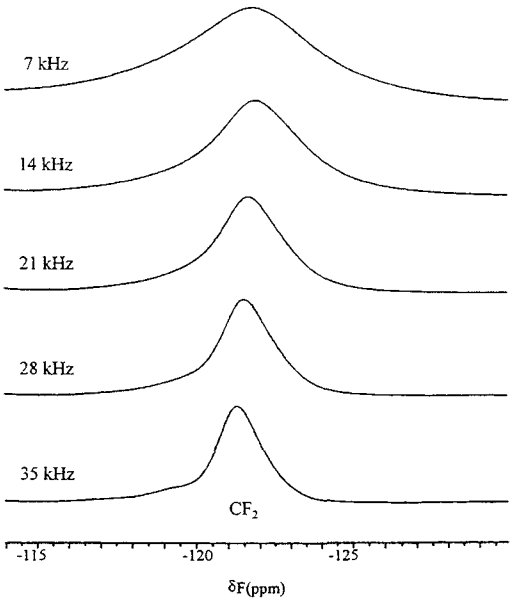

Fig. 2: CF_2 region of the spectra in Fig. 1

In Fig. 2 a zoom of CF_2 signal from the tetrafluoroethylene is depicted. This series of spectra illustrates the line narrowing with increasing spinning frequency. The line width in fluorine spectra of systems with abundant fluorines is determined by both the anisotropy of the chemical shift, which is inhomogeneous, and the dipolar coupling, which is homogeneous. The resulting interaction in this case is homogeneous as well [4], which means that the linewidth of both the isotropic lines and the sidebands is inversely proportional to the spinning frequency [5, 6]. The inhomogeneous line broadening due to a distribution of chemical shifts plays a minor role here as can be seen in the spectrum recorded at 35 kHz.

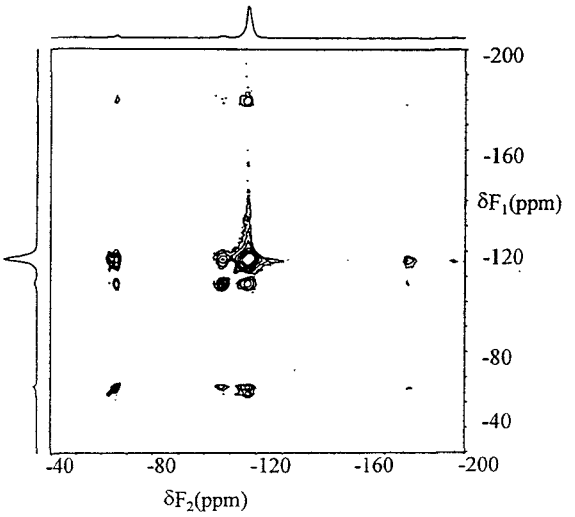

Fig. 3: Fluorine-19 RFDR spectrum of FEP. MAS frequency 25 kHz, t_m=1 ms.

Fig. 3 shows a spin exchange spectrum of the FEP used for the spectra in Fig. 1, which has been recorded using radio frequency driven recoupling (RFDR) [7]. In this experiment high-speed MAS is applied to record high-resolution solid-state NMR spectra during the evolution and the detection period. During the mixing time a sequence of rotor-synchronized π pulses is applied to reintroduce the homonuclear dipolar coupling. The π pulses in addition refocus the evolution under chemical

shift for every rotor period, thus enabling a very efficient spin exchange, because there is no frequency difference.

The spin exchange is determined by the direct dipolar coupling, the coupling through space, and therefore the exchange intensity is a measure of the distance between the exchanging spins. This can be utilized for the assignment of the signals. Although no through bond correlation like in J-coupled spectra [8, 9] is measured, because the distances between fluorines at the same polymer chain are much shorter than the distances between fluorine nuclei at different chains. The correlations in Fig. 3 indicate, that the signal at –112 ppm originates CF_2 from the hexafluoropropylene units.

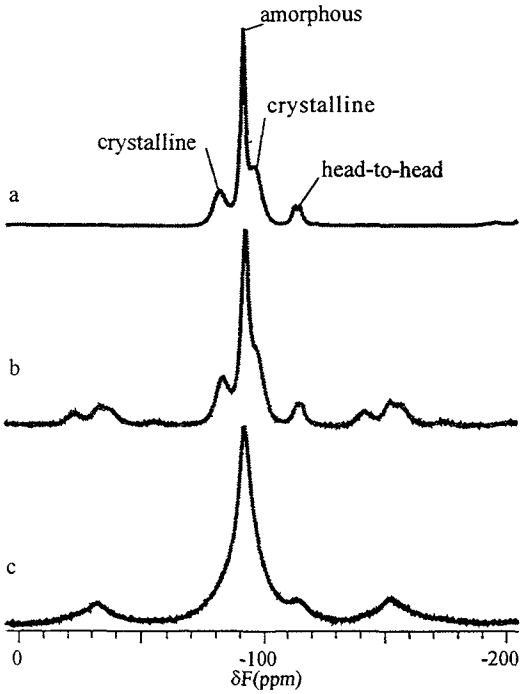

Fig. 4: Fluorine-19 MAS NMR spectra of PVDF. a) 32 kHz no proton decoupling, b) 16 kHz with proton decoupling, c) 16 kHz no proton decoupling.

In Fig. 4 MAS spectra of PVDF (polyvinylidenedifluoride) are depicted. Although the structure of PVDF is rather simple, the spectrum is complicated because it is semicrystalline. The two signals at –89 ppm and –99 ppm originate from the crystalline part of the polymer and the one at –92 ppm from the amorphous part and the ones at –115 ppm from head-to-head polymerizations [10]. The spinning speed of 32 kHz in Fig. 4a is sufficient to average both the homonuclear and the heteronuclear dipolar coupling. In Fig. 4b and Fig. 4c a spinning frequency of 16 kHz has been applied. While in Fig. 4c without proton decoupling the resolution is poor and the spectral features are invisible, in Fig. 4b under high-power proton decoupling the different lines are resolved, although the line width is bigger than in the spectrum in Fig. 4a due to the homonuclear coupling. In the decoupled spectrum no correction for Bloch-Siegert [11] shift has been applied, because the effect here is below 1 ppm.

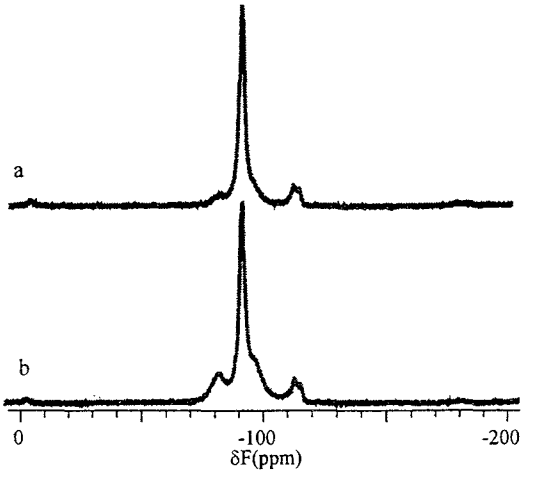

Fig. 5: Fluorine-19 MAS spectra of PVDF, a: REDOR spectrum with a mixing time of 0.4 ms or 10 rotor cycles. b: spin echo spectrum as reference

Fig. 5 shows two MAS spectra of the PVDF sample, which indicate the possibility to select magnetization. In Fig. 5a) a REDOR-type [12] spectrum with a mixing time of 0.4 ms or 10 rotor cycles is shown, Fig. 5b shows a spin echo spectrum with the same number of cycles. The suppression of the signals from the crystalline part in the REDOR spectrum can

clearly be seen. This suppression results from the much stronger heteronuclear dipolar coupling in the crystalline part compared to the weaker coupling in the amorphous part. In this way REDOR-type experiments can be used as magnetization filters similar to [13] as well.

An RFDR spectrum of PVDF for a mixing time of 4 ms, in this case 128 rotor cycles, is depicted in Fig. 6. Strong exchange signals can be seen between the two signals originating from the crystalline part of the polymer which proves the strong coupling in the crystalline part and the spatial proximity of the two types of fluorines. The exchange between the amorphous and the crystalline part is much weaker. The head-to-head polymerizations show exchange peaks only to the signal from the amorphous part. There is no cross peak to the crystalline part of the polymer, which proves that the head-to-head polymerizations are located in the amorphous part of the polymer. This result is in good agreement with results from proton-fluorine wideline separation experiments [13].

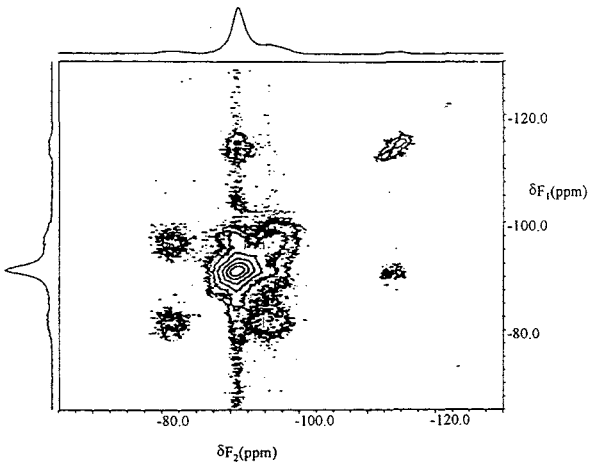

Fig. 6: Fluorine-19 RFDR spectrum of PVDF, MAS frequency 32 kHz, mixing time 4 ms. The grey bars indicate the spin exchange.

In addition two signals from the head-to-head polymerizations can be distinguished in the solid-state spectra as well. The fact that there is no significant exchange between these two signals, means that these signals originate from different types of head-to-head polymerizations which are separated in space.

Acknowledgement

I wish to thank Dr. U. Lappan (IPF) for the FEP sample, Dr. P. Holstein (University of Leipzig) for the PVDF and helpful discussions. Financial support by the Deutsche Forschungsgemeinschaft (DFG) is gratefully acknowledged.

References

[1] P. Jackson, R.K. Harris, Chem. Rev. 91, (1991), 1427

[2] U. Scheler, R.K. Harris, Chem. Phys. Lett., 262, (1996), 137

[3] U. Scheler, Solid-state NMR, 12, (1998), 9

[4] M. Mariq, J.S. Waugh, J. Chem. Phys. 70, (1979), 3300

[5] E. Brunner, D. Fenzke, D. Freude, H. Pfeiffer, Chem. Phys. Lett. 169, (1990), 591

[6] S. Hafner, H.W. Spiess, Concepts in Magn. Reson., 10, (1998), 99

[7] A.E. Bennett, J.H. Ok, R.G. Griffin, J. Chem. Phys. 96, (1992), 8624

[8] A. Lesage, C. Auger, S. Caldarelli L. Emsley, J. Am. Chem. Soc. 119, (1997), 7867

[9] M. Baldus and B. H. Meier, J. Magn. Reson. A 121, (1996), 65

[10] P. Holstein, U. Scheler, R.K. Harris, Polymer, 39, (1998), 4937

[11] S. Vierkötter, J. Magn. Reson. A118, (1996), 84

[12] T. Gullion, J. Schaefer, J. Magn. Reson., 81, (1989), 196

[13] U. Scheler, R.K. Harris, Solid-State NMR 7, (1996), 11

EPR Investigation of Structural Phase Transition in layered $KTm(MoO_4)_2$.

E.N. Khatsko, M.I. Kobets and Ju.V. Pereverzev.
Institute for Low Temperature Physics and Engineering of National Academy of Science of Ukraine.
310164 Kharkov, Ukraine.

Investigation of low-dimensional systems, such as rear-earth double molybdates is of interest for number of reasons. A strong anisotropy and competition of one-ion and different-ions anisotropy leads to peculiarities in energy spectrum of magnetic ion. A presence of considerable magnetic moment in rare-earth ion and rather small exchange interaction raise a role of dipole-dipole interaction. And finally in these low symmetric magnetic crystals an essential lattice instability is noted as result of electron and phonon subsystems interconnection and existence of degenerated or quasi- degenerated ground state of magnetic ion. As a result a variety of phase transitions is observed, not only magnetic but structural (including cooperative Jahn-Teller type), ferroelectric and ferroelastic too. Phase transitions (among them structural ones) in these systems can be induced not only by the temperature but by the magnetic field as well.

This paper is concerned with the EPR investigation of $KTm(MoO_4)_2$ compound. This layered crystal belong to the family of double alkali rare-earth molybdates.

$KTm(MoO_4)_2$ refers to the rhombic space group symmetry $D^{14}{}_{2h}$[1]. The lattice constant are: a = 18.31 A, b = 7.89 A, c = 5.05 A. The unit cell contain four molecules. The rare-earth ions form chains along *b* axis and the separation between ions is about 3.9 A. For Tm^{3+} in the ground state is $^3H_6$ with the lowest singlet level. But the first exited state on evidence derived from our microwave absorption date is very close and distant less than 3 cm^{-1}.These two layers form quasi-doublet. The next state is spaced several tens of cm^{-1}. This scheme is confirmed by temperature dependence of magnetic susceptibility of the single crystal of $KTm(MoO_4)_2$, studied down to 1.8 K. There is smooth maximum in 150 K region caused by «freezing» of high levels and then there is no evidence of susceptibility lowering up to the lowest temperature realized in experiment.

High frequency properties of $KTm(MoO_4)_2$ was studied at temperatures ranged from 1.8 K to 35 K at frequency range from 11 to 190 GHz in permanent magnetic field up to 8 T. The polarization of *hf* magnetic field was perpendicular to the external magnetic field direction. The angular dependencies of the EPR spectra of lowest quasi-doublet of Tm^{3+} ion was studied in three main crystallographic plane of the crystal. Two nonequivalent position of Tm^{3+} was found rotated in plane *bc* on the angle $\theta = \pm 7.6^\circ$ with respect to *b*-axis with highly anisotropic ground level g-factor. A frequency-field dependence of absorption line along *b*-axis shows nonlinear behavior. It is quite well described by quadratic in magnetic field low $\omega^2=\omega_0{}^2+(g_bH/2)^2$ with a gap ω_0 = 69.95 GHz and g_b= 13.9. This correlates with energy gap in zero magnetic field $\Delta E \cong 2.5$ cm^{-1}. Along *a* and *c* axes g-factors are less then 0.4. Thus it is valid to say that $KTm(MoO_4)_2$ belong to the Ising magnets.

At temperature 1.8 K when the external magnetic field is applied along *c*-axis of crystal (the smallest g-factor in *bc*-plane) under the forward and reverse magnetic field varying a drastic modification of the absorption line is observed in fields from 30 to 40 kOe (see fig.1). A considerable hysteresis ($\Delta H \approx 5$ kOe) is noted. An additional peculiarity in low field about 7 kOe is observed too. As the temperature increases above 2 K the anomalies in absorption disappear. The microwave frequency was varied from 18 to 120 GHz and the position of these peculiarities do not depend on the frequency at a

given constant temperature. It follows that observed peculiarities are not electron paramagnetic resonance but are due to a phase transition, evidently 1st kind type. As the magnetic field is declined in bc-plane from the c-direction the hysteresis phenomenon is observed in a narrow range of angles of magnetic field deviation from c-axis of crystal. On further declination of magnetic field the peculiarities remain but without the hysteresis.This appears that first kind of transition give way to the second one.

The differential magnetic susceptibility *dM/dH* was measured in temperature interval 1.8 K-4.2 K for a magnetic field orientation along the *c*-axis of crystals (Fig.2). Likewise the absorption spectra an anomaly in the field dependence of *dM/dH* is observed too. At temperatures below 2 K a jump of *dM/dH* is noted in magnetic field about 40 kOe. A remarkable hysteresis something like 4 kOe occur in magnetic field passing forth and back. These anomalies vanish as the temperature increases higher than 2 K. The *dM/dH*(H) dependence demonstrates jumps of susceptibility both in field nearly 30 kOe and in low field about 7 kOe. Just as the high field anomaly so the low field one display distinct hysteresis under changes of field direction.

The observed peculiarities cannot be understand in frame of EPR. At first because of its independence from microwave frequency, and second due the hysteresis phenomena. They cannot be explained as a purely magnetic phase transition reorientation type «drawn» by the magnetic field, because as foloows from susceptibility measurements in $KTm(MoO_4)_2$ there are no magnetic ordering down to 0.3 K while observed feature take place up to 2 K.

The strong spin-orbit interaction, orbital degeneracy or quasi-degeneracy and as result the lattice instability suggest that a first-order Jahn-Teller structural phase transition induced by external magnetic filed can occur. But in this scheme the two lowest Kramers doublet levels are needed, while in $KTm(MoO_4)_2$ lowest quasi-non Kramers doublet is significantly separated from next exited also non Kramers doublet level.

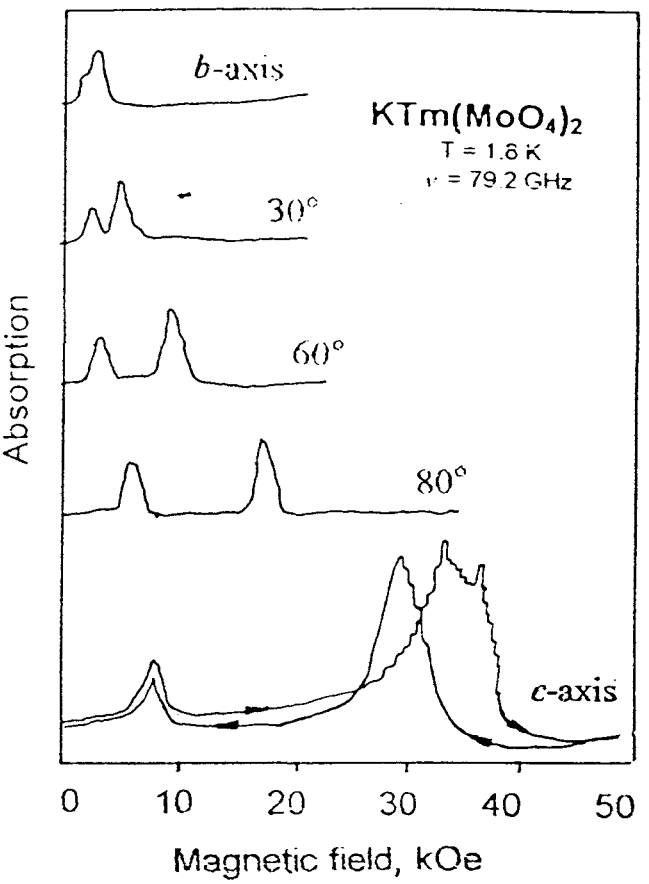

Fig.1 Field dependence of absorption spectrum in $KTm(MoO_4)_2$ for different magnetic field directions in ac-plane at T=1.8 K The arrows indicate the direction of magnetic field deviation.

Our interpretation of phenomenon is based on assumption that anomalies in microwave absorption and susceptibility arise in vicinity of structural phase transitions forced by external magnetic field. In the construction of model of these phase transitions we start from the next suppositions. In all crystals under investigation the nearest ligand environment of a magnetic ion (complex) is mainly responsible for the configuration of its crystal field and strong anisotropy of magnetic properties. The exited levels are separated from ground level by a wide gap and are not taken into account in the further

consideration. We suppose that the complex has a rigidity in the sense that it can be turned as a whole in the *bc*-plane without a change in the principal values of the g-tensor. When magnetic field is applied along the smallest g-factor in *c*-direction the system will gain in the magnetic energy, if the crystal will be distorted so that the g-factor component in magnetic field direction will be increased. This is realized by rotation of complex. Clearly we loss in elastic energy. The rotation of interacting complex become profitable in strong enough magnetic fields (the magnetic analog of Jahn-Teller effect).

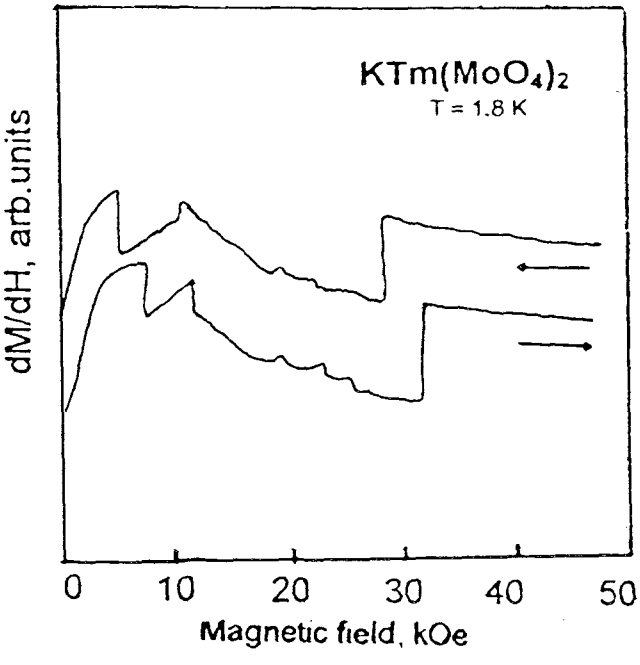

Fig.2. Field dependence of differential magnetic susceptibility *dM/dH* of $KTm(MoO_4)_2$ for H|||c at T=1.8 K The arrows indicate the direction of magnetic field deviation.

By this means the initial Hamiltoian [2] is defined as a sum of three terms: the term which describes the interaction of the rotating degrees of freedom of complexes, one-ions potential energy of complex with three-well potential, and finally, the Zeeman term, which entangle the rotating degree of freedom of complexes with the spin degree of freedom of rare-earth ion. The phase H-T diagram of this model have a complicated view dictated by the magnitude of one-ion anisotropy. The diagram involves both the first kind phase transition lines and second kind ones too. In this instance the constant of one-ion anisotropy is a function of the three-well potential characteristic,the magnitude of magnetic field, and an angle of magnetic field deviation from symmetric direction. At present the fit of experimental data to theoretic ones in order to obtain a parameters of initial model is carried out.

So the totality of experimental data analysis shows that observed anomalies in absorption spectra are due to a structural phase transition of 1^{st} kind induced by applied magnetic field.

Conclusions

The angular and frequency depedences of EPR spectra of single crystals of $KTm(MoO_4)_2$ were studied at helium temperatures. It was shown that this compound belong to the Ising magnets with strong anisotropy of spin interactions.

1.The g-factors of ground quasi-doublet have been determined: $g_a = >0.4$; $g_b = 13.9$; $g_c = >0.4$.

2.Two magnetic non-equivalent position of Tm^{3+} ions in $KTm(MoO_4)_2$ crystal lattice was identified. The angle of the unroll of local magnetic axes of two centeres $2\theta = 15.2^{\circ}$ was found.

3. The splitting of ground state of Tm^{3+} ion in $KTm(MoO_4)_2$ $\Delta E \cong 2.5\ cm^{-1}$ was determined.

4. Magnetic field induced 1^{st} kind structural phase transition was found in single crystal of $KTm(MoO_4)_2$. This phase transition occurs when permanent magnetic field is applied along *c*-axis of crystal at temperatures lower than 2 K. The explanation is founded on competition of elastic energy and magnetic one in in case of strongly anisotropic g-factors.

1. V.I. Spicin and V.K. Trunov, *Rep. of Ac. Of Sc. Of USSR*, **183**, 129, (1968).
2. Yu.V. Pereverzev, *Low Temp.Phys.*, **22**, 226, (1996).

Calendar of Forthcoming Conferences in Magnetic Resonance

May 22-28, 1999
Seventh Scientific Meeting and Exhibition of the Intl. Soc. for Magnetic Resonance in Medicine (ISMRM), Philadelphia, Pennsylvania (USA)

For information contact:

ISMRM
2118 Milvia St.
Suite 201
Berkeley, CA 94704

May 25 - June 5, 1999
International School of Structural Biology and Magnetic Resonance, 4th Course: Dynamics, Structure and Function of Biological Macromolecules, Erice, Sicily (Italy)

For information contact:

Ms. Robin Holbrook
Stanford Magenitc Resonance Laboratory
Stanford University
Stanford, CA, 94305-5055 Phone: (650) 723-6270
Fax: (650) 723-2253
E-mail: reh@stanford.edu

May 30 - June 5, 1999
8th Chianti Workshop on Magnetic Resonance, Nuclear and Electron Relaxation, San Miniato (PISA), (Italy)

For information contact:

Ivano Bertini
University of Florence
Department of Chemistry
Via Gino Capponi 7
50121 Firenze - Italy
Fax: +39-055-2757555
E-mail: chianti@lrm.fi.cnr.it

June 6-11, 1999
Gordon Research Conference on: Computational Aspects of Biomolecular NMR, Conference Center "Il Ciocco", Barga (Italy)

For information contact:

Gordon Research Conferences
University of Rhode Island
P.O. Box 984
West Kingston, Rhode Island 02892-0984 USA
Phone: (401) 783-4011
Fax: (401) 783-7644
E-mail: GRC@grcmail.grc.uri.edu
E-mail: app@grcmail.grc.uri.edu (send/request e-mail application)
Registration http://www.grc.uri.edu

June 14-18, 1999
Specialized Colloque AMPERE
EPR, NMR, NQR in Solid State Physics - Recent Trends, Pisa (Italy)

For information contact:

Conference Secretariat, IFAM-CNR, Via del Giardino, 7
56127 Pisa Italy
Fax: +39 50 3139035
E-mail: ampere@ifam.pi.cnr.it

June 27 - July 2, 1999
14th International Meeting on NMR Spectroscopy, Royal Society of Chemistry, University of Edinburgh, Edinburgh (U.K.)

For information contact:

Dr. John Gibson
The Royal Society of Chemistry
Burlington House
Piccadilly
London
W1V 0BN
United Kingdom
Phone: +44 (0) 171 437 8656 Fax: +44 (0) 171 734 1227 E-mail: conferences@rsc.org

July 10-15, 1999
NMR in Molecular Biology - Structure, Binding and Molecular Recognition, Granada, (Spain)

For information contact:

Dr. Josip Hendekovic
Phone: +33 3 88 76 71 35
Fax: +33 3 88 36 69 87
E-mail: clemoal@esf.org

August1-5, 1999
41st Rocky Mountain Conference on Analytical Chemistry, Denver, Colorado (USA)

For information contact:

Phone: 1-800-996-3233
E-mail: milestone@bod.net

August 6-7, 1999
Varian/Chemagnetics 10th Annual Workshop on Solid State NMR, Estes Park, Colorado (USA)

For information contact:

Jim Frye
Chemagnetics/Varian NMRI
2607 Midpoint Dr.
Ft. Collins, CO 80525 USA
Phone: (888) VARIANS or (970) 493-7007 x244
Fax: +1-970-482-0570
E-mail:

August 14-19, 1999
37th IUPAC Congress, Frontiers in Chemistry: Molecular Basis of the Life Sciences, Gesellschaft Deutscher Chemiker, Berlin (Germany)

For information contact:

Gesellschaft Deutscher Chemiker
IUPAC 99
P. O. Box 90 04 40
D-60444 Frankfurt am Main, Germany
Phone: +49-69-7917-358/ -360/ -366
Fax: +49-69-7917-475
E-mail: tg@gdch.de
Homepage: http://www.gdch.de

September 12-16, 1999
The Alpine Conference on Solid-State Nuclear Magnetic Resonance, Chamonix-Mont Blanc (France)

For information contact:

Alpine Conference Secretariat
Laboratoire STIM
Ecole Normale Superieure de Lyon
46, Allee d'Italie
69364 Lyon cedex 7, France

April 9-14, 2000
41st ENC (Experimental NMR Conference), Asilomar Conference Center, Pacific Grove, California (USA)

For information contact:

ENC
1201 Don Diego Avenue
Santa Fe, NM 87505 (USA) Phone: (505) 989-4573
Fax: (505) 989-1073 E-mail:
enc@enc-conference.org

The editor would be pleased to receive notices of upcoming meetings in the field of magnetic resonance to include in future volumes.